Pan-cancer Screening of Optimal Combinations with novel ONN, BAQ13

By

CLAIRE ELIZABETH JACOBSEN
THESIS

Submitted in partial satisfaction of the requirements for the degree of

MASTER OF SCIENCE

in

Pharmacology and Toxicology

in the

OFFICE OF GRADUATE STUDIES

of the

UNIVERSITY OF CALIFORNIA

DAVIS

Approved:

_____

Yuanpei Li, Chair

_____

Kermit Carraway

_____

Jeremy Chien

Committee in Charge

2023

Abstract

Cancer's position as the second leading cause of death in the United States as well as the prevalence of treatment resistance highlights the need for new, more efficacious treatment strategies. For this reason, our lab has integrated nanotechnology with initial drug design and developed a one-component new-chemical-entity nanomedicine (ONN) strategy to improve both the potency and delivery kinetics of cancer therapeutics. Bisaminoquinolone 13 (BAQ13) is one of a series of self-delivering ONNs that has shown efficacy in lysosomal disruption and dysfunction as well as autophagy inhibition (3). To combat different types of treatment resistance we investigated BAQ13's ability to combine with ferroptosis inducers, Paclitaxel (PTX), and radiation as well as its role in the modulation of fatty acid oxidation (FAO) and lipid toxicity. To carry out these experiments we employed methods such as viability assays (MTS and CellTiterGlo), clonogenic assays, an FAO assay kit, confocal microscopy, and western blots. As will be discussed, BAQ13 had potential in combination with ferroptosis inducer Erastin but not RSL3 with further investigation of the BAQ13 – Erastin combination potentially implicating other cell death pathways. BAQ13 also did not consistently synergize with Paclitaxel, despite multiple attempts with different dose ranges and treatment paradigms including 24- or 72-hour pretreatments. In terms of FAO, BAQ13 was observed to downregulate and potentially inhibit FAO activity at higher doses and those same higher doses led to lipid toxicity via lipid droplets, lipid bilayer disorder, and phospholipidosis. Lastly, combination of BAQ13 and radiation proved especially efficacious and synergistic in cells possessing intrinsic and acquired radioresistance and a more widespread screen revealed synergy in other cell lines. Overall, BAQ13 has the potential to be very effective in combination treatment, especially as a strategy to lessen or prevent treatment resistance.

List of Figures

Table of Contents

Introduction

Cancer is the second leading cause of death in the United States with 1.9 million new cancer cases and over 600,000 deaths in 2022. Standard of care for cancer treatment usually includes chemotherapy, radiotherapy, surgery, or some combination of the three. However, nanomedicine, an emerging field in cancer therapeutics, has risen to improve drug-intrinsic kinetics and safety profiles, though this carries some limitations of its own; complexity and toxicity, patent issues, and inability to modify certain drug structures. Our lab has therefore sought to integrate nanotechnology into initial drug design to develop a one-component new-chemical-entity nanomedicine (ONN) strategy (Fig. 1). This involves conventional drug design strategies alongside molecular self-assembly so that the drugs have advantages in drug discovery as well as drug delivery (3). Additionally, conventional chemotherapeutics typically target and induce

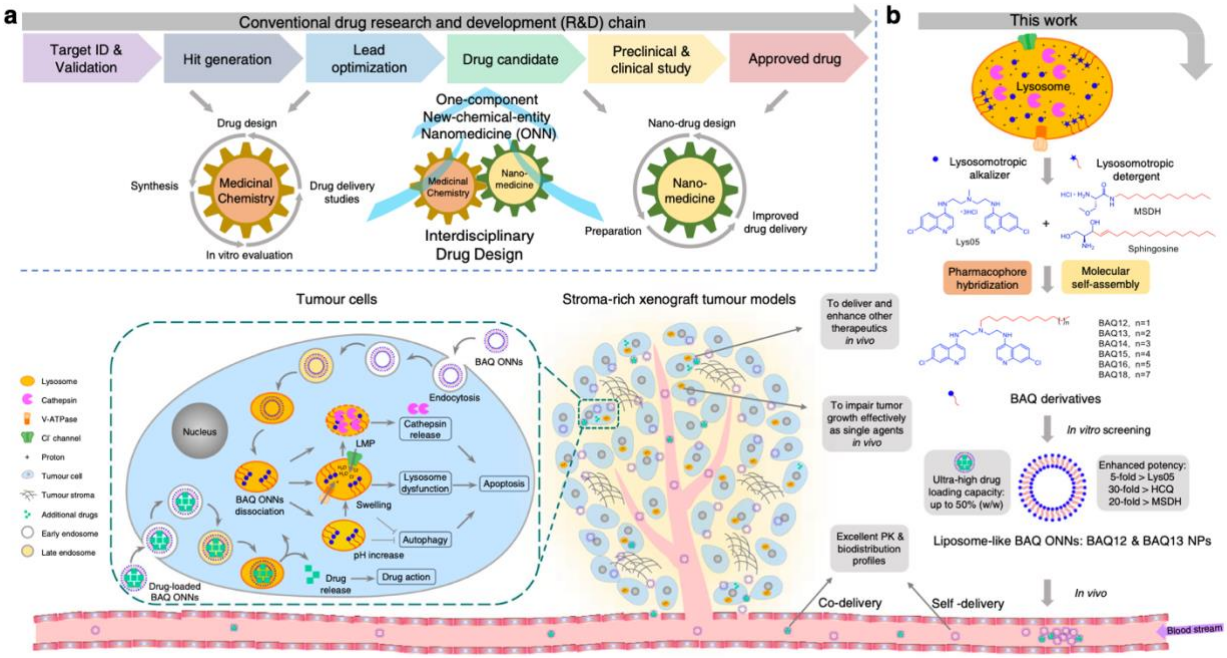

Figure 1. Schematic illustration of BAQ13's drug design strategy, molecular targets, and anticancer potential. Ma et al. 2020.

apoptosis, which is commonly met by treatment resistance. This led our lab to choose lysosomes as a therapeutic cancer target as cancer cell lysosomes are more fragile due to hypertrophy and

easy rupture. Lysosomal membrane permeabilization (LMP) can directly trigger cell death through the release of proteolytic enzymes into the cytoplasm. In addition, lysosomal inhibition interferes with autophagy which plays a significant role in the cellular stress response and treatment resistance (3).

Autophagy is a pathway involving the engulfing of cytoplasmic components through autophagosomes for presentation to lysosomes leading to degradation. The main purpose of this process is to maintain cellular homeostasis and health and it is regulated mainly by the phosphatidylinositol 3-kinase (PI3K) – protein kinase B (AKT) – mechanistic target of rapamycin complex 1 (mTORC1) pathway (Fig. 2). Radiotherapy can induce either protective autophagy or autophagic cell death, each resulting from different cellular triggers. DNA damage and large amounts of reactive oxygen species (ROS) lead to cytoprotective autophagy which results in the removal of damaged mitochondria, reduction in oxidative stress, and improved tumor cell radioresistance. However, some studies have found that radiation can also terminate tumor cell self-renewal, blocking cell division and stimulating autophagic cell death (4).

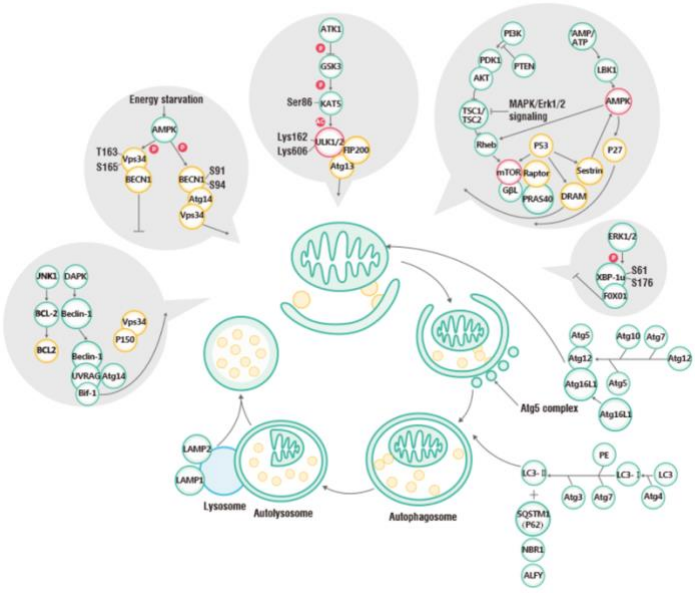

Figure 2. Summary schematic of the different components making up each step of the autophagy pathway. Antibodies.com

Bisaminoquinolone 13 (BAQ13)

Cancer's prevalence as well as its position as the second leading cause of death in the United States highlights a need to improve current treatments. BAQ13 is one of a series of self-delivering ONNs that has shown high efficacy in lysosomal disruption, lysosomal dysfunction, and inhibition of autophagy with a 30-fold higher antiproliferative effect compared to its parent compound hydroxychloroquine (3). Each of the BAQ entities were also specifically equipped with improved drug delivery properties and tumor-targeted biodistribution, a main reason for their significant anticancer effects both *in vitro* and *in vivo*. Ma et al. (3) also discovered an unintended property of BAQ13; the nanoparticle drug has the capacity for drug loading, opening the possibility for synergism and delivery of an additional drug. BAQ13's ability to block autophagy thus presents a way around protective autophagy and instead a strategy to trigger autophagic cell death, enhancing anticancer efficacy of each treatment.

This project will bring together a unique combination of techniques for measuring cell proliferation and thus the anticancer efficacy of various BAQ13 combinations. Using our lab's chemical and biological expertise, these combinations will be formulated and tested. The *in vitro* efficacy of mono- and combination treatments will be determined, optimal combinations will be narrowed down, and a pan-cancer screen will be performed on the most efficacious combination. Knowledge will be contributed regarding autophagy's role in various combinations as well as radiation resistance and the degree to which targeting this resistance mechanism lessens the development or persistence of treatment resistance. This treatment strategy should open possibilities for other combinations with other compounds, namely autophagy inhibitors, to further enhance efficacy and eventually improve clinical outcomes. In addition to overcoming treatment resistance and enhancing anticancer efficacy, this work is also likely to lead to

improved toxicity profiles for each treatment.

Short term implications of our work include improved targeting of a portion of a complicated resistance mechanism to better target tumors that have intrinsic or developed treatment resistance. Aside from the scientific contributions, this project will reveal a network of techniques and background knowledge that can be used for future studies with BAQ13. Thus, this study will provide an optimized experimental approach to screening and analysis of synergistic treatment combinations. Our results, both immediate and for future studies building upon this one, will improve the prognosis of resistant cancers, prevent development of said resistance, increase target specificity and antitumor efficacy, and reduce toxicity associated with each treatment.

Ferroptosis

Ferroptosis is a more recently discovered cell death pathway driven by lethal lipid peroxidation (21). This form of cell death is a consequence of cellular metabolism and imbalanced redox homeostasis and can be suppressed by blocking lipid peroxidation directly or through depleting iron pharmacologically or genetically. As the name implies, there is a requirement for iron in this form of cell death with it also relying on ROS and phospholipids with polyunsaturated fatty acid chains. The initiation mechanisms of lipid peroxidation are not fully understood but are thought to occur through both enzymatic and non-enzymatic processes in 3 phases: initiation, propagation, and termination. As a part of this process, Fenton reactions utilize iron and oxygen to catalyze a chain reaction forming phospholipid hydroperoxides which, if not rapidly cleared, can react with labile iron to generate radicals, forming more hydroperoxides (21).

There are multiple ways in which ferroptosis can be suppressed to promote the survival of cancer cells. First is uptake of cysteine followed by glutathione or thioredoxin reductase-dependent reduction of cysteine and GSH biosynthesis. GSH is a potent reductant/cofactor for glutathione peroxidase 4 (GPX4) which allows for GPX4 mediated reduction of phospholipid hydroperoxides. Next is the ferroptosis suppressor protein 1 (FSP1) – ubiquinone system that completely protects cells against ferroptosis induced by the inhibition or deletion of GPX4. FSP1 is able to prevent lipid peroxidation and thus ferroptosis through reducing ubiquinone to ubiquinol or eliminating the radical form of vitamin E. Lastly, other ferroptosis-suppressive mechanisms include squalene-mediated and di/tetrahydrobiopterin-mediated inhibition of lipid peroxidation through acting as endogenous radical-trapping antioxidants (21).

As mentioned in the paper by Jiang et al. (2021), ferroptosis is regulated through lipogenesis, iron, and redox homeostasis. Lipogenesis is required for lipid peroxidation and ferroptosis and leads to production of phospholipids with polyunsaturated fatty acid chains. Iron import via transferrin and autophagy-mediated ferritin degradation both promote ferroptosis. Lastly, imbalanced redox homeostasis occurs due to cells lacking reducing agents such as cysteine leading cellular metabolism to cause an accumulation of ROS, contributing to ferroptosis. Ferroptosis has also been thought to play a role in tumor suppression via p53 as it can increase ferroptosis through suppressing the transcription of the system responsible for cysteine uptake (21). The tumor suppressor and epigenetic regulator BAP1 can also increase ferroptosis through similar mechanisms. However, p53 has also been reported to prevent ferroptosis through altering its other transcriptional targets, illustrating that the role of ferroptosis in tumor suppression is still incompletely understood.

Logically, cancer cells should have a higher tendency to undergo ferroptosis due to higher metabolism and ROS production. Additionally, cancer cells also often require more iron and may also possess mechanisms to counter burdens that will reduce their susceptibility to ferroptosis. It has also been determined that cells that are resistant to apoptosis or common cancer therapeutics are highly susceptible to ferroptosis inducers as the malignant mutations driving metastasis and protecting cells from apoptosis may sensitize them to ferroptosis. Additionally, tumor cells undergo sustained oxidative stress and are more dependent on cysteine uptake for ROS detox, conveying greater vulnerability to cysteine system inhibition than normal tissues (21). All of this makes ferroptosis an attractive target for cancer treatment, especially for combination therapy. Jing et al. (22) demonstrated that ferroptosis contributes to the cytotoxic effects of cisplatin. Combination treatment with dihydroartemisinin (DHA) demonstrated synergism likely driven by DHA reinforcing mitochondrial ROS production with cisplatin treatment. This synergy is also due in part to ferroptosis as accumulation of lipid peroxides was observed prior to cell death and accumulation of labile free iron was accelerated. It was also speculated that cisplatin could induce GSH depletion and GPX4 inactivation which can lead to ferroptosis. This was confirmed through use of ferroptosis inhibitor DFO which lessened ferroptotic cell death while addition of Fe^{2+} accelerated it. All of this is to say that ferroptosis could eliminate the resistance of cancer cells to drug-induced apoptosis as cisplatin resistant cells have been shown to have increased vulnerability to ferroptosis (22).

Paclitaxel

Taxanes, such as paclitaxel and docetaxel, are a well-known and widely used class of cancer therapeutics, especially for tumor types including ovarian, breast, head and neck, lung, and prostate cancer (32). For the purposes of this line of research, the focus will be on paclitaxel

(PTX) which has a mechanism of action based on the stabilization of microtubule fibers which hinders the function of the mitotic spindle thereby inducing cell cycle arrest and cell death, likely via apoptosis (31). However, a limitation of PTX is that resistance could develop via multiple mechanisms. These mechanisms include increased expression of the multidrug resistance (MDR) phenotype, alterations of the cellular target (i.e., tubulin and the microtubule system), and a more novel mechanism: PTX-induced cytoprotective autophagy (31, 32).

BAQ13 has been established as an autophagy inhibitor as evidenced by the large amount of preclinical data demonstrating the ability to modulate this process both *in vitro* and *in vivo* (3). Thus, to combat PTX resistance, it is prudent to investigate the effects of combination treatment with BAQ13. Autophagy plays an important role at the onset of PTX resistance (31) making this combination treatment necessary for the prevention of resistance rather than its reversal. As mentioned previously, BAQ13 is derived from compounds such as chloroquine which has shown promise in phase II clinical trials when co-administered with PTX for treatment of metastatic breast cancer (31). Additionally, hydroxychloroquine (HCQ) combined with nab-PTX was able to reduce autophagy levels in pancreatic cancer demonstrated by increased SQSTM1 protein expression (31). This combination's efficacy was further supported by improved tumor response indicating that combination with an autophagy inhibitor is promising for pancreatic cancer, which is the primary cancer type in which BAQ13's efficacy was initially showcased (3).

However, *in vitro* combination treatment with PTX proves difficult as it's mechanism of cell cycle arrest leads the drug to be more cytostatic rather than cytotoxic. This is a limitation in the sense that traditional viability assays such as MTS and CellTiter Glo are rendered ineffective as the cells are still alive and metabolically active but are unable to divide. Therefore, it is necessary to investigate different dosing schemes and pre-treatments. This includes simultaneous co-

treatment with 24–72-hour incubation, 24–72-hour pre-treatment with PTX before treatment with BAQ13 for another 24 hours, and pre-treatment with BAQ13 for 24 hours before treatment with PTX for 72 hours. An additional method worth investigating is 72-hour treatment with PTX followed by removal of the drug and any dead cells and addition of BAQ13 for an additional 24 hours. These approaches will allow us to exhaust any and all possibilities for synergy with this combination, providing a thorough screening of this treatment strategy.

Fatty Acid Oxidation

Metabolic reprogramming is one of the hallmarks of carcinogenesis and tumor progression seen through increased glycolysis in solid tumors. Despite this, metabolism is often not a static process, especially if cells are under any kind of genotoxic stress. Mitochondrial oxidative respiration can be adjusted to meet energy consumption needs for fueling cell cycle progression and DNA repair (13). However, the role of mitochondrial fatty acid β-oxidation (FAO) in cancer is not completely understood. FAO is one of the major sources of ATP production (Fig. 3), but most other studies of cancer bioenergetics have not focused on it, with building evidence that abnormal FAO activity is linked to oncogenesis. Various cancer cells rely on FAO for proliferation, survival, stemness, drug resistance, or metastasis (23). Therefore,

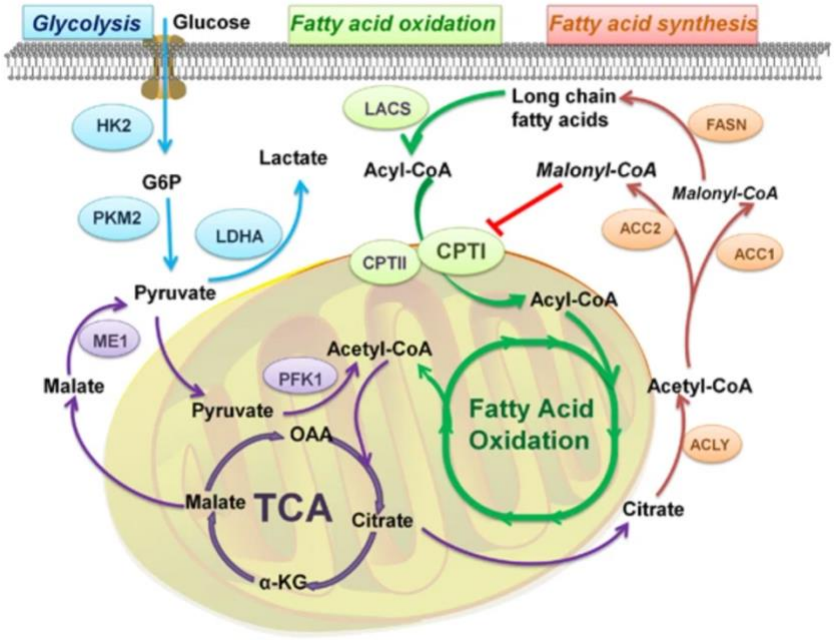

Figure 3. Metabolic pathways including glycolysis and FAO highlighting key regulators such as CPT1 (30).

FAO, namely its key enzymes and regulators, have become promising targets for cancer therapy and potentially combination treatment. Fatty acid oxidation is a multistep catabolic process allowing for mitochondrial conversion of long chain fatty acids into acetyl-CoA which will then be oxidized through the TCA cycle and electron transport chain (ETC) to produce ATP (23). Key enzymes and regulators include carnitine palmitoyltransferase (CPT1), of which CPT1A is most likely to be enzymatically active in cancer cells exhibiting high lipogenesis and FAO, and peroxisome proliferator-activated receptors (PPARs) that act as environmental fat sensors and transcriptional activators of FAO enzymes (23).

Constant, systemic treatment of cancer will unavoidably lead to drug resistance, hindering the efficacy and curative capacity of many cancer therapies. Studies have shown that FAO activation is a mechanism by which cancer cells can develop drug resistance in response to treatments such as dexamethasone (25), imatinib (26), rapamycin (27), and tamoxifen (28), to name a few. Therefore, it is worth exploring the ability of BAQ13 to manipulate the FAO pathway in addition to investigating possible synergy between BAQ13 and FAO inhibitor Etomoxir.

As mentioned above, CPT1 is a key regulator of FAO, leading it to be identified as a potential therapeutic target for cancer treatments. In certain cancers such as breast, prostate, glioblastoma, colon, and others, CPT1 expression is increased with CPT1 inhibition having antitumor effects (29). The specific function of CPT1 is the transfer of a long chain acyl group from coenzyme A to carnitine which is required to transport long-chain fatty acids into the mitochondrial matrix for oxidative degradation via FAO. Etomoxir is a drug commonly used to inhibit CPT1 in cancer studies and has been shown to impair nicotinamide adenine dinucleotide phosphate (NADPH) production and increase ROS, leading to ATP depletion and cell death (30).

Treatment with Etomoxir has additionally been shown to not only inhibit cancer cell proliferation but also sensitize cells to apoptosis, hinting at an ability to combat treatment resistance (30). Therefore, it is worth investigating the ability of Etomoxir to synergize with BAQ13 as alone, both have promise to circumvent treatment resistance.

Radiotherapy and Radiation Resistance

Cancer affects millions of Americans, with the probability that 1 in 2 people will develop some form of cancer during their lifetime. Of this number, over half receive radiation as part of their cancer treatment and unfortunately, at least 20 percent discover that their tumors are resistant to radiotherapy. Radioresistance is associated with various biological alterations of tumor cells and the tumor microenvironment that result in modulation of cell fate decision leading to escape from death and increased proliferation (4). Currently, there is a clinical need for identifying optimal radiotherapy – drug combinations to both improve treatment efficacy and combat resistance (5).

Modulation of multiple forms of cancer cell death in parallel with the prevalence of radioresistance make radiation a promising candidate for combination therapy. Specifically, radiotherapy is one of the stresses that induces autophagy-mediated survival in cancer cells although the mechanism linking the two has not been fully elucidated (2). Therefore, use of an autophagy inhibitor in combination with radiotherapy presents a strategy to both combat radioresistance and more effectively inhibit cancer cell growth. This project aims to validate and optimize the combination of radiation and autophagy inhibition using BAQ13. We hypothesize that targeting autophagy and lysosomal disruption using BAQ13 will present an effective combination with radiotherapy by inhibiting the survival mechanisms that radiation alone

induces. Characterizing this combination will eventually allow for clinical translation and a major step in overcoming radioresistance.

Radiotherapy plays a crucial role in cancer treatment with the common treatment regimen of standard fractionated irradiation; 1.8-2 Gray (Gy) per day, 5 days a week to limit side effects and toxicity to normal tissues, although exceptions exist if it is possible to deliver higher doses of radiation in a field confined to the tumor tissue (6). While radiotherapy is increasingly common, so is radioresistance which is accompanied by dysregulation of various cell death pathways including autophagy. Activation of autophagy, a process that maintains cellular energy levels, has been shown to contribute to cancer development and promote treatment resistance with autophagy inhibition enhancing radiation-induced apoptosis in many types of cancer cells (7). Han et al. (2014) demonstrated that direct inhibition of autophagy led to a significant increase in cell death through radiation-induced apoptosis and suppression of the TAK1 kinase. Thus, the outcome of this study was the overcoming of established radioresistance using autophagy inhibitors to block radiation-induced TAK1 activation. Additionally, it has been shown that lysosome-targeted inhibition of autophagy with BAQ13 precursors chloroquine and hydroxychloroquine or knockdown of lysosome-related genes is able to sensitize cells to radiotherapy (8). Therefore, the preceding data provides a solid foundation for investigating the hypotheses proposed here regarding autophagy and lysosomal disruption using BAQ13 in combination with radiation to overcome radioresistance in a variety of cancer types.

Radiotherapy's effectiveness in terms of killing cancer cells is dependent on the type of radiation, total dose, fractionation rate, and the target. Alone, this therapy can be effective in treating certain types of cancer such as larynx cancer, non-small-cell lung cancer, skin cancer, prostate cancer, cervical cancer, head and neck carcinomas, and lymphomas. On the other hand,

it is not always effective in cancers such as breast cancer, bladder cancer, glioblastoma, soft tissue carcinoma, and advanced non-small-cell lung cancer potentially due to intrinsic radioresistance (1). Thus, whether radiation resistance is intrinsic or acquired, it presents a significant obstacle in the treatment of many cancers. Therefore, one of the fundamental and incompletely resolved issues regarding radioresistance is how to sensitize resistant cell lines to radiotherapy. As previously discussed, lysosome-targeted autophagy has shown promise as a method by which to overcome radioresistance through the accumulation of autolysosomes (8) although this has not been extensively investigated with different types of radioresistance across multiple cell lines.

Methods

Cell culture: Procedures were executed as published in (3). All cell lines were cultured and passaged according to ATCC guidelines.

Cell viability: For cell viability assays, 3,000-5,000 cells per well of 96-well plates were seeded and dosed within 24 hours and incubated with BAQ13 and/or other compounds at 37 ℃ for 48 hours. At the end of this period, MTS solution or CellTiter-Glo were administered and incubated according to established protocols (2-4hrs for MTS, 15min for CellTiter-Glo) before reading absorbance or luminescence and calculating percent viability.

Colony formation/Clonogenic assay: For colony formations, we seeded 1,000-5,000 cells per well of 6-well plates or 5cm plates and dosed with BAQ13, radiation, or both within 24 hours and incubated at 37 ℃ for 7-15 days before staining with crystal violet and counting the number of colonies similar to procedures published in (13) with subsequent calculations of combination indices via Combenefit software.

Combenefit: A detailed explanation of the rationale behind this software can be found in (36). Cell viability or clonogenic assay data was entered into this software as follows; all treatment groups were divided by the untreated control value and multiplied by 100 to get a viability percentage. Then, the data was entered into one of the templates on the software's website so it could be placed directly into the Combenefit software. Upon running the data through the software, we collected data from each of the classical models for synergy: Loewe, Bliss, and Highest Single Agent (HSA). The output from this consists of single agent dose response data, combination dose response, model-generated reference combination dose response, and synergy distribution.

Radiation: For radiation only and combination colony formations cells were dropped off (after seeding 1,000-2,000 cells/well the previous day) in a 37 ℃ incubator in Research II for radiation which can only be performed by members of the Jian Jian Li Lab. The cells were exposed to radiation for varying amounts of time with increasing time correlating with increasing doses of radiation (Gy). After radiation, the cells were picked up within 24 hours from the same incubator and placed in our lab's incubator where they were left undisturbed for 7-15 days.

Confocal imaging: Seeding and dosing were completed as published previously (3). We also stained and imaged the cells using LipiORDER, LipidTOX, LipiDYE-M, and FAOBlue dyes as published in (14), (15), (16), and (35), respectively using both 20X and 63X oil lens objectives of a Zeiss confocal fluorescence microscope located in Research I. The procedures for each dye are outlined below.

LipiORDER: 1μM LipiORDER was prepared in Hank's Balanced Salt Solution (HBSS). Cells were seeded overnight at 15,000 cells/well and the next day were dosed with media (untreated), BAQ13, or ETX overnight. On the day of imaging, culture medium was removed and the cells were gently washed one time with Phosphate Buffered Saline (PBS) before the addition of the LipiORDER-containing medium. The dye was then incubated for at least 10 minutes before removing and washing gently with PBS once. Before imaging, 100uL Live Cell Imaging Buffer (HBS) was placed in each well.

LipidTOX: 1000X LipidTOX reagent was diluted 1:500 in normal growth medium in order to create a 2X solution. Cells were seeded overnight at 15,000 cells/well and the next day medium was removed for addition of 50uL/well 2X LipidTOX reagent and 50uL/well media (untreated) and 2X concentrations of BAQ13 and ETX before overnight incubation. On the day of imaging, culture medium was removed and 100uL 4%

formaldehyde was added to each well and incubated for 30 minutes. After the incubation period, the fixed cells were washed gently with PBS once to remove excess formaldehyde. Before imaging, 100uL PBS was placed in each well.

LipiDYE-M: 5μM LipiDYE-M was prepared in HBSS. Cells were seeded overnight at 15,000 cells/well and the next day were dosed with media (untreated), BAQ13, or ETX overnight. On the day of imaging, culture medium was removed and the cells were gently washed one time with PBS before the addition of the LipiDYE-M-containing medium. The dye was then incubated for 6 hours before removing and washing gently with PBS once. Before imaging, 100uL Live Cell Imaging Buffer (HBS) was placed in each well.

FAOBlue: 10μM FAOBlue was prepared in HEPES-buffered saline (HBS). Cells were seeded overnight at 15,000 cells/well and the next day were dosed with media (untreated), BAQ13, or ETX overnight. On the day of imaging, culture medium was removed and the cells were gently washed one time with HBS before the addition of the FAOBlue-containing medium. The dye was then incubated for at least 30 minutes before removing and washing gently with HBS once. Before imaging, 100uL Live Cell Imaging Buffer (HBS) was placed in each well.

Fluorescence Quantification: A numbered workflow for this process can be found in (37). Fluorescent images were placed into ImageJ Fiji for analysis. Parameters were set according to published instructions and cells/areas of interest were outlined with the freehand tool before analyzing by choosing 'measure' yielding several measurements including area, mean, and integrated density. 5 representative areas were chosen on images with too many cells to count whereas oil lens images only had about 5 cells per image. Therefore, for background

measurement, 5 representative background areas with no fluorescence were chosen for analysis. Then, the mean fluorescence of background readings was calculated. To calculate corrected total cell fluorescence (CTCF) the following equation was used for all images/treatment groups: Integrated density – (Area of selected cell x Mean fluorescence of background readings). This data was then averaged within each treatment group and for each dye the data was placed into a bar graph for comparison between groups with specific data sets for red, green, and merged channels where applicable.

Western blot: As published previously (3), this procedure was performed as part of screening pancreatic cancer cells (MiaPaCa-2) to assess cell death pathways behind the Erastin – BAQ13 combination.

FAO assay: This assay was carried out as published previously (13). PANC-1 and MiaPaCa-2 cells were seeded at 650,000-750,000 cells/well of six well plates and dosed with varying doses of BAQ13 and Etomoxir with different incubation periods in order to visualize both dose- and time- dependent differences in FAO activity. As collection methods are unspecified in the published protocol, we have found that scraping after the addition of lysis buffer to be the most efficient method to collect the cells without great loss of protein. Other than this note we followed the published protocol, using the included reagents.

Results

Pharmacological Manipulation of Ferroptosis in Combination with BAQ13

There are various ways to pharmacologically induce ferroptotic cell death as was mentioned above. Two well-known ferroptosis inducers are Erastin which activates p53 to induce ferroptosis, and RSL3 which triggers ferroptosis by directly inhibiting GPX4. These two ferroptosis inducers were highlighted as having potential to combine with autophagy inhibitor BAQ13 to enhance cancer cell death. Initial experiments were completed using Erastin in combination with BAQ13 in MiaPaCa-2 cells with visible synergy at high doses of each drug (Fig. 4). However, replicating these results proved difficult leading to a shift in experimental design. Thus, subsequent experiments were run using RSL3 which required significantly lower concentrations than Erastin. RSL3 demonstrated some synergy but results were again inconsistent, leading to troubleshooting and repeat experiments with expanded dose ranges and exposure time. Subsequent attempts, representative image seen in

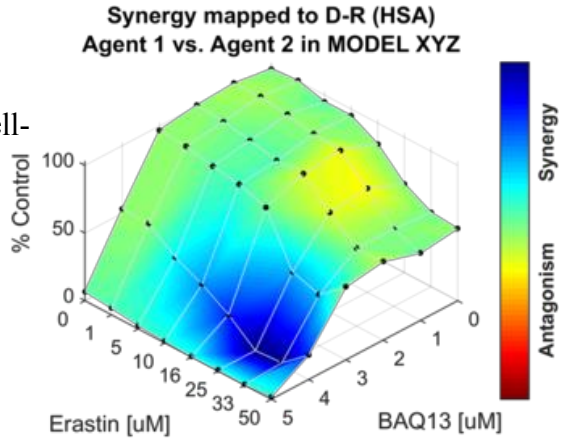

Figure 4. HSA synergy of BAQ13 combined with Erastin for 24 hours in MiaPaCa-2 cells.

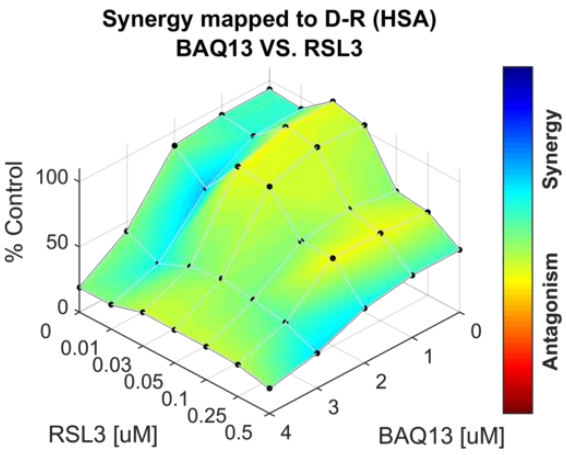

Figure 5. Attempt 1 of RSL3 vs. BAQ13 combination

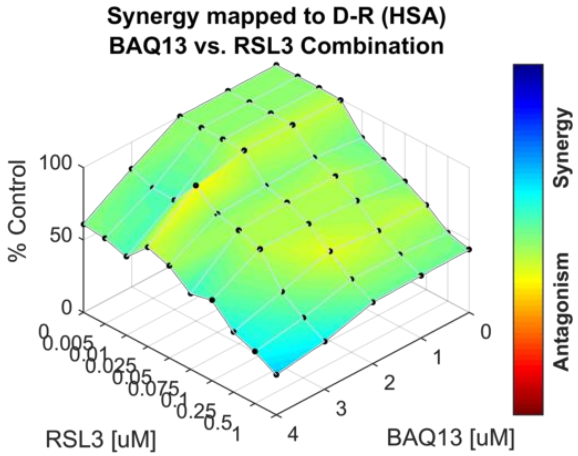

Figure 6. Attempt 2 of RSL3 vs. BAQ13 combination

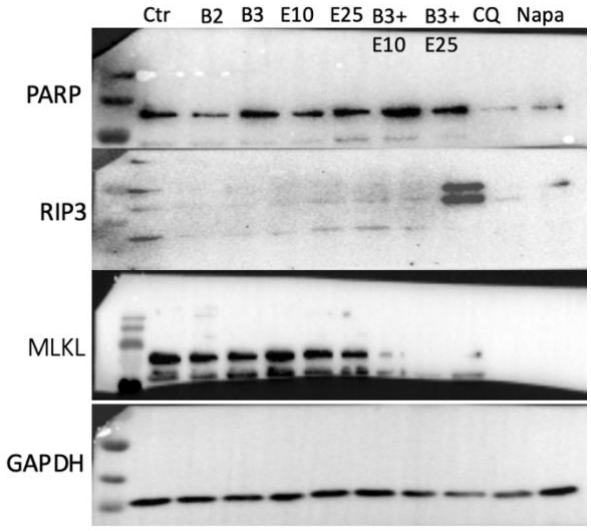

Figure 7. Representative Western blot images prbing for markers of various cell death pathways.

Figures 5 and 6, demonstrated similar inconsistency with some synergy seen at the highest μM concentrations. The synergy potential seen with Erastin then led to running of Western blots (Fig. 7) after dosing for 6-24 hours to visualize the various cell death pathways involved in combination treatment. The combination treatment mainly demonstrated an effect on apoptosis and necrosis markers with upregulation of RIP3 and downregulation of MLKL, a seemingly contradictory result as RIP3 is a regulator of MLKL. Regarding apoptosis, combination treatment led to cleavage of PARP with no notable modulation of other apoptotic markers such as caspase 3 (data not shown). Lastly, expression of housekeeping protein GAPDH was equal across all treatment groups. All of this presents interesting preliminary data suggesting a possible synergistic combination of BAQ13 and Erastin with some evidence of interaction of autophagic, ferroptotic, apoptotic, and necrotic cell death mechanisms. Further study should focus on elucidation of specific cell death mechanisms to more accurately map out the synergism seen with Erastin and investigate why the same synergism was not seen with RSL3. Variability that could have contributed to the irreproducibility of results include freeze/thawing of samples in addition to BAQ13's lack of stability in solution above 4 degrees Celsius or when exposed to excessive light.

Paclitaxel-BAQ13 Combination to Address Autophagic Resistance Mechanisms

Pancreatic cancer cells inherently possess elevated levels of autophagy, making them more prone to developing resistance to treatments such as standard of care chemotherapies like Paclitaxel

(PTX). For this experiment PANC-1 and MiaPaCa-2 cells were used and first treated with PTX alone with concentrations ranging from 0-10μM. This did not yield a traditional IC_{50} perhaps due to the fact that PTX is cytostatic rather than cytotoxic despite literature establishing IC_{50}s of 34 nM and 21 nM for PANC-1 and MiaPaCa-2 respectively (33). This led us to investigate the synergistic potential of BAQ13-PTX combination treatment in both pancreatic cancer cell lines. Initially, 4 attempts were completed in MiaPaCa-2 cells with simultaneous co-treatment of BAQ13 and PTX, none of which showed significant synergistic effects that could be replicated (Fig. 8). Throughout each attempt, the BAQ13 doses were kept constant, ranging from 0-4μM with some modulation of PTX concentrations and treatment for 72 hours. The most synergy was seen with the highest concentration of PTX (10μM) which could not be replicated. The inconsistency

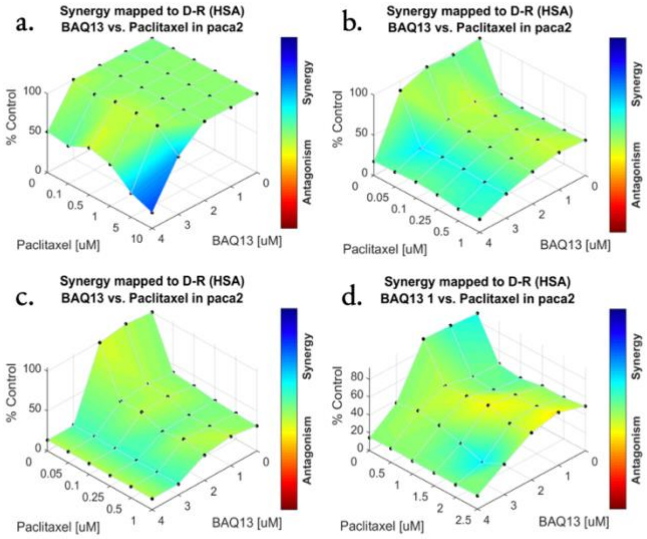

Figure 8. Combenefit HSA synergy plots of simultaneous co-treatment of BAQ13 and PTX for 72 hours in MiaPaCa-2 cells.

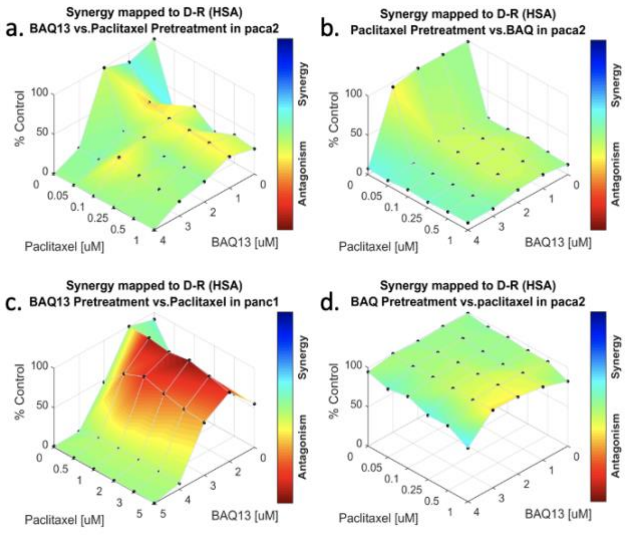

Figure 9. Combenefit HSA synergy plots of 24 hour pretreatment with PTX (a, b) and BAQ13 (c, d) in MiaPaCa-2 cells.

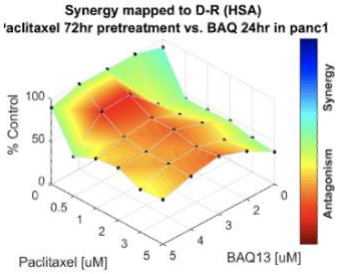

Figure 10. Combenefit HSA synergy plot of 72 hour PTX pretreament followed by 24 hour BAQ13 treatment in MiaPaCa-2 cells.

then led to different treatment paradigms including 24- and 72-hour pretreatment with each drug which yielded similar results (Fig. 9, 10). Therefore, there is little to no observable synergy with the PTX-BAQ13 combination in MiaPaCa-2 cells with some antagonism seen with BAQ13 pretreatment. For PANC-1 cells, 3 initial attempts were completed with simultaneous co-treatment of BAQ13 and PTX which showed mild synergy at higher doses (Fig 11), prompting the investigation of 24- and 72-hour pretreatment (Fig. 12, 13) with each drug to determine if stronger synergy could be achieved. While some synergy was seen with 24-hour PTX pretreatment (Fig. 12a, b), each attempt was marked by mild to significant antagonism. Thus, combination treatment with BAQ13 and PTX in PANC-1 cells is, at best, weakly synergistic and potentially antagonistic depending on the treatment schedule. The preceding data demonstrates a clear lack of consistent or strong synergy with this combination despite alterations in dose and treatment schedule. Further study of this

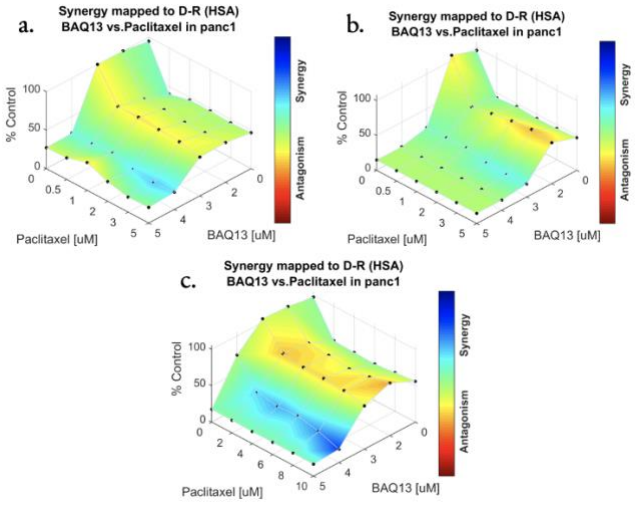

Figure 11. Combenefit HSA synergy plots of simultaneous co-treatment of BAQ13 and PTX for 72 hours in PANC-1 cells.

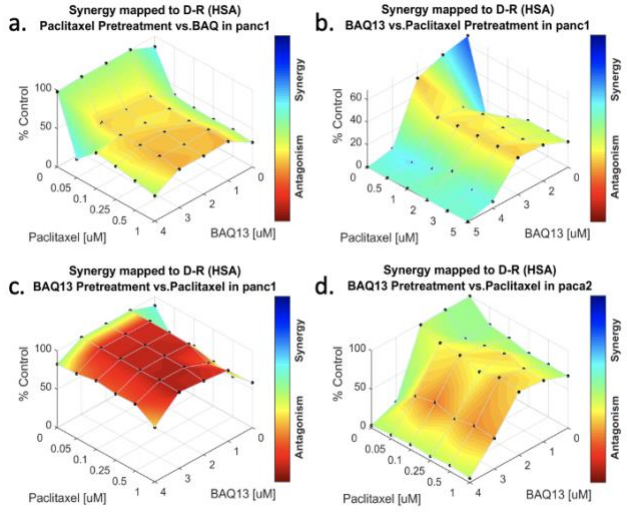

Figure 12. Combenefit HSA synergy plots of 24 hour pretreatment with PTX (a, b) and BAQ13 (c, d) in PANC-1 cells.

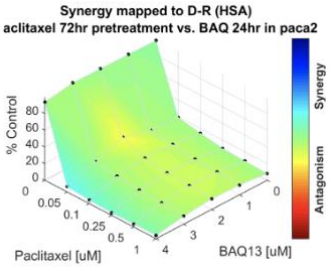

Figure 13. Combenefit HSA synergy plot of 72 hour PTX pretreament followed by 24 hour BAQ13 treatment in PANC-1 cells.

combination could include mechanistic studies of each compound alone and of combination treated cells as well as expansion to other cancer types with different levels of susceptibility to PTX and/or autophagy inhibition by BAQ13.

BAQ13's Manipulation of Metabolism and Lipid Toxicity

Fatty Acid Oxidation

BAQ13's cytotoxicity via autophagy inhibition has been demonstrated both by preceding experiments and publications (3), which led to questions about other potential mechanisms behind its efficacy. Changes in metabolism, specifically FAO activity, is an established method to visualize the pathophysiologic and metabolic basis of many diseases. Therefore, using an FAO assay kit from University at Buffalo, State University of NY we measured dose- and time-dependent changes in FAO activity upon treatment with BAQ13 in PANC-1 and MiaPaCa-2 cells in order to determine the metabolic effects, if any, BAQ13 possesses. For the following bar graphs, each bar represents one data point per attempt hence the lack of error bars and data points. The first attempt (Fig. 14) was irregular and showed no trends with increasing dose or time, likely due to inconsistent or low protein concentrations in each sample due to a flawed collection method (washing rather than scraping cells). Subsequent attempts were collected via

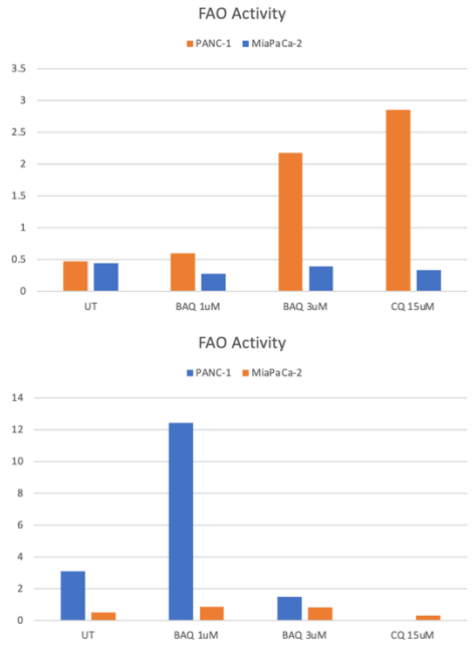

Figure 14. Initial FAO attempt with 24-hour treatment in MiaPaca-2 (p2) and PANC-1 (p1) cells.

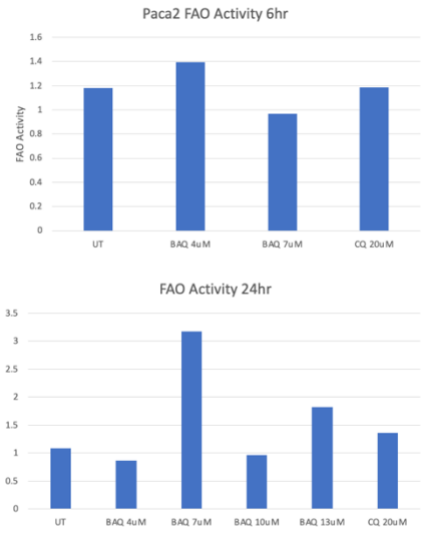

Figure 15. Results of FAO attempts with 6- and 24-hour treatment in MiaPaCa-2 cells.

scraping and yielded better protein concentrations but with many doses still low or out of range (assay requires 1-3mg/mL of protein). Due to further inconsistencies in protein levels, the results were still relatively irregular but suggestive of a trend of sorts; FAO activity seems to peak at the middle (7μM) dose for 24-hour treatment but with 6-hour treatment, the peak appears at the lower (4μM) dose for MiaPaCa-2 (Fig. 15) with no notable trends in PANC-1 cells other than a peak seen in Figure 14 at a 2μM dose (higher doses were unavailable along with 6-hour treatment for PANC-1 at this time due to low protein concentrations). For PANC-1 cells a 4-hour treatment was added as a method to troubleshoot low protein concentrations potentially due to excess cell death with longer treatment periods. This revealed a trend similar to what has been discussed with MiaPaca-2 cells with a peak at the low (5μM) dose and a subsequent "crash" at the high (8μM) dose. There were many inconsistencies with this line of experimentation so further study should focus on streamlining this assay or expanding to other cell lines and assays to more accurately determine if and how BAQ13 enacts metabolic dysfunction.

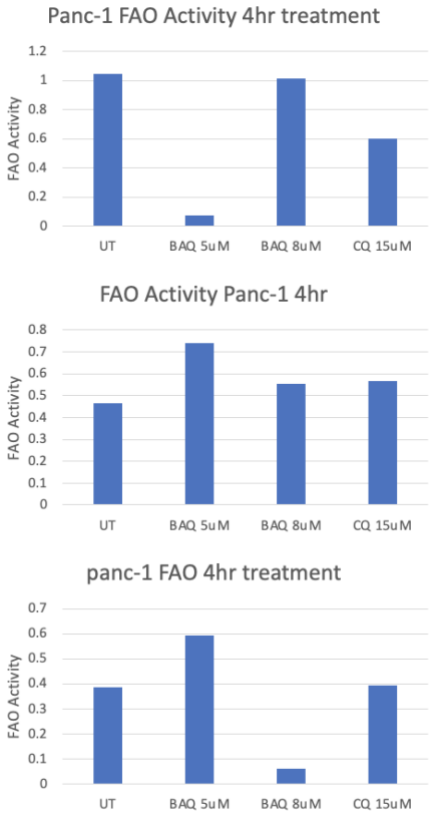

Figure 16. Results of FAO attempts with 4-hour treatment in PANC-1 cells.

Combination with FAO inhibitor Etomoxir

To further visualize modulation of FAO activity, we utilized the effects of FAO inhibitor Etomoxir (ETX) alone and in combination with BAQ13. We began by treating PANC-1 and MiaPaCa-2 cells with ETX concentrations ranging from 100-600μM which yielded an IC_{50} of

300-400μM which is in line with published literature citing use of ETX at concentrations ranging from 40-200μM (34). Combination treatment with BAQ13 reduced the viability of the pancreatic cancer cells at 100-200μM ETX concentrations at BAQ13 doses of 1-5μM. The lack of a significant combination effect led us to utilize ETX's inhibitory effect on FAO activity as a negative control for FAO Blue fluorescent dye in PANC-1 cells. This dye will exhibit increased blue fluorescence corresponding to increased FAO activity (35). Initially, we imaged cells in 4 treatment groups overnight: untreated, 2μM BAQ13, 3μM BAQ13, and 200μM ETX. This initial attempt confirmed the same trend discussed in the previous section with FAO activity increasing at the 2μM concentration compared to a "crash" at 3μM with no activity seen in the ETX group (Fig. 17). Subsequent attempts with higher BAQ13 doses (5 and 8μM) showed a similar trend with the "crash" at the higher BAQ13 dose resembling the untreated control (Fig. 18).

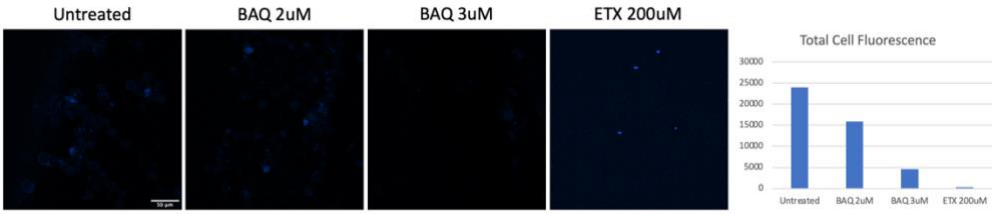

Figure 17. Representative images of MiaPaCa-2 cells stained with FAOBlue dye with increased blue fluorescence corresponding to increased FAO activity. Fluorescence is quantified in the accompanying graph.

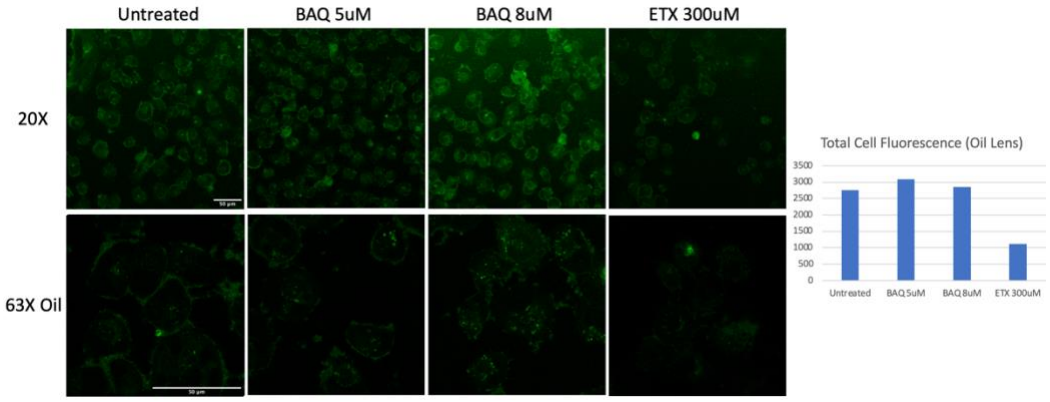

Figure 18. Representative images of MiaPaCa-2 cells stained with FAOBlue dye (green) with increased green fluorescence corresponding to increased FAO activity. Fluorescence is quantified in the accompanying graph.

Lipid Toxicity

To visualize the potential for BAQ13 to induce lipid toxicity we utilized various fluorescent dyes. LipiDye-M is a novel fluorescent dye-labelled C12 fatty acid that senses environmental polarity and in response changes absorption and fluorescent spectrum (16). This dye exhibits red fluorescence in lower polarity and green fluorescence in higher polarity and can also change colors in intracellular environments such as the cytosol (green), organelle membranes (yellow), and lipid droplets (red). Treatment groups were similar to the preceding section (higher BAQ13 doses: 5μM and 8μM), again in PANC-1 cells, and demonstrated that higher BAQ13 doses led to increased lipid droplet formation indicating increased lipid toxicity (Fig. 19). ETX showed moderate increase in lipid droplets or polarity compared to the untreated control. Morphological changes in the cells were unable to be discerned because PANC-1 cells do not have an extensive cytoplasm, making visualization of specific organelles by fluorescent color very difficult. To further investigate lipid toxicity, we utilized fluorescent dye LipiORDER. This dye allows for visualization of membrane lipid order via changes in fluorescence with green indicating low polarity and an ordered, thick lipid bilayer and red indicating high polarity and a disordered, thin lipid bilayer (14). Intermediate colors between red and green (i.e., light green, yellow, orange) indicate varying levels of disorder and thus, level of lipid toxicity these cells are experiencing. Again, higher doses of BAQ13 led to increased disorder and low polarity as

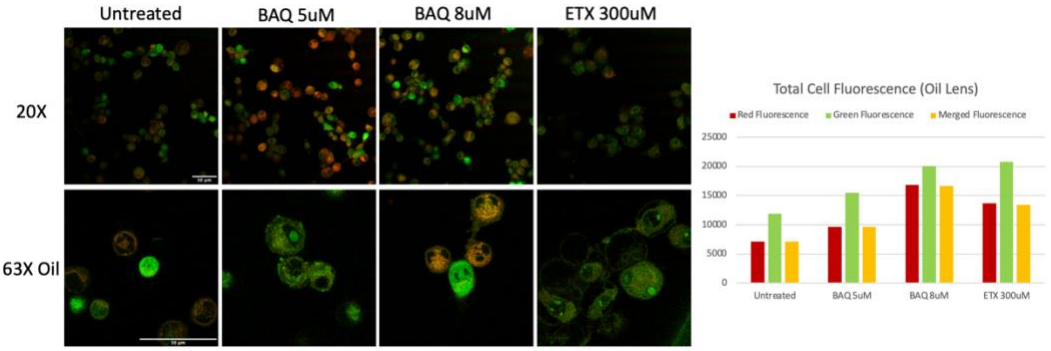

Figure 19. Representative images of PANC-1 cells stained with LipiDye-M showing cytosol and mitochondrial matrix (green), organelle membranes (yellow), and lipid droplets (red). Fluorescence is quantified in the accompanying graph.

evidenced by a dose-responsive increase in red color (Fig. 20). The ETX treated group also had some disorder but was more balanced, similar to the untreated control, albeit with lower overall fluoresence. Lastly, we utilized LipidTOX fluorescent dye developed to characterize the potentially toxic side effects of compounds on lipid metabolism in mammalian cell lines (15). Specifically, this dye detects phospholipidosis which is often triggered by cationic lipophilic drugs and can be detected in cells incubated in the presence of phospholipids conjugated to fluorescent dyes (15). In this case, increased green fluorescence indicates a stronger presence of phospholipidosis. The images and quantification (Fig. 21) confirmed what was seen with the previous dyes with increased BAQ13 concentrations leading to increased green fluorescence, especially when compared with the untreated control. For this dye, the ETX group appeared to mimic the untreated control with a slightly lower degree of green fluorescence. Overall, these experiments demonstrate that BAQ13 is able to manipulate metabolic processes in addition to its capacity to induce various forms of lipid toxicity. Future investigations should mechanistically outline these abilities to provide a greater understanding of all of BAQ13's cytotoxic effects.

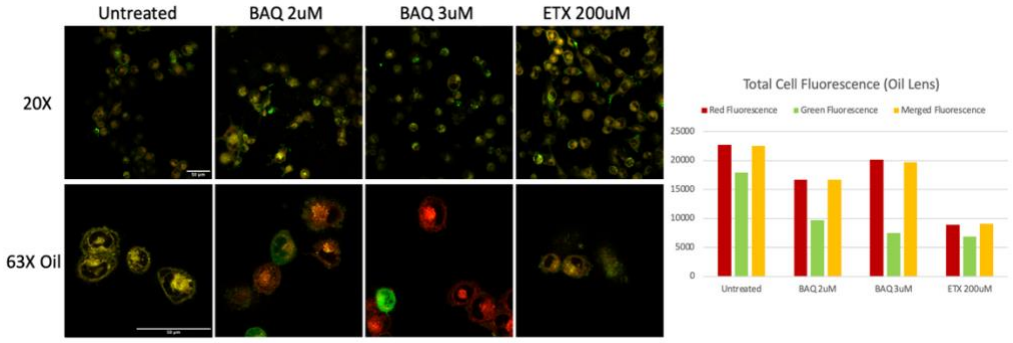

Figure 20. Representative images of PANC-1 cells stained with LipiORDER showing low polarity, ordered lipid bilayers (red) and high polarity, sparse/disordered lipid bilayers (green) with yellow showing an intermediate degree of order. Fluorescence is quantified in the accompanying graph.

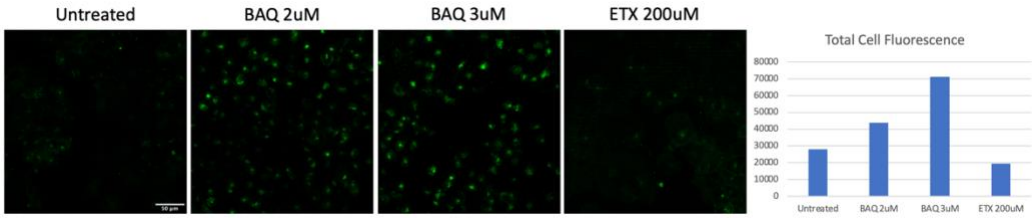

Figure 21. Representative images of PANC-1 cells stained with LipidTOX dye which shows increased green fluorescence with increased levels of phospholipidosis. Fluorescence is quantified in the accompanying graph.

BAQ13 and Radiotherapy Combination to Combat Radioresistance

Pancreatic Cancer

As mentioned before, pancreatic cancer is accompanied by increased levels of autophagy, which translates to intrinsic radioresistance. Therefore, due to BAQ13's anticancer potential being showcased in pancreatic cancer cells (3) we began to investigate the potential for BAQ13 to prevent or reverse radioresistance in combination treatment. Initial experiments measuring acute (24-72 hour) effects of radiation resulted in negligible toxicity, leading us to pursue colony formations to assess chronic toxicity instead. Acute BAQ13 IC_{50}s were ~2-3μM for MiaPaCa-2 and ~3-5μM for PANC-1 cells which we utilized to determine a lower dose range for chronic

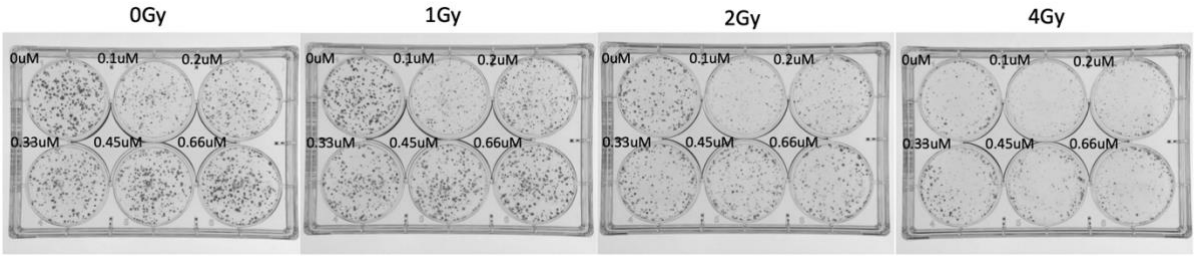

Figure 22. Representative images of clonogenic assays in PANC-1 cells treated with a combination of BAQ13 and radiation.

toxicity studies. After conducting initial experiments to determine chronic IC_{50} values for both BAQ13 (0.1-0.66μM) and radiation (2-8Gy) in PANC-1 and MiaPaCa-2 cells, we began combination treatment. Based on initial characterization the cells were treated with the same concentrations of BAQ13 and slightly lower radiation doses (1, 2, and 4Gy). This revealed a somewhat dose-responsive trend with increasing doses of BAQ13 and radiation, especially in PANC-1 cells, representative image seen in Figure 22, with the HSA synergism plot (Fig. 23) indicating moderate synergism with increasing doses of both radiation and BAQ13. Bliss and Loewe

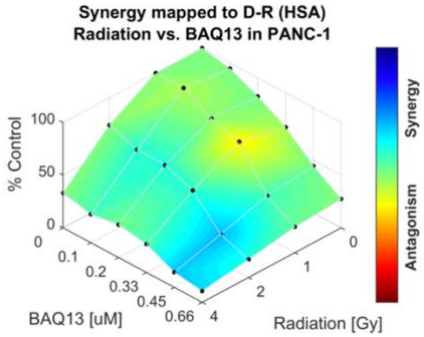

Figure 23. HSA synergy plot of the results of combination treated colony formation assays in PANC-1 cells.

synergy models had similar results (data not shown) with Bliss showing slightly less synergy and Loewe showing synergy in a similar spot with some antagonism at lower doses. MiaPaCa-2

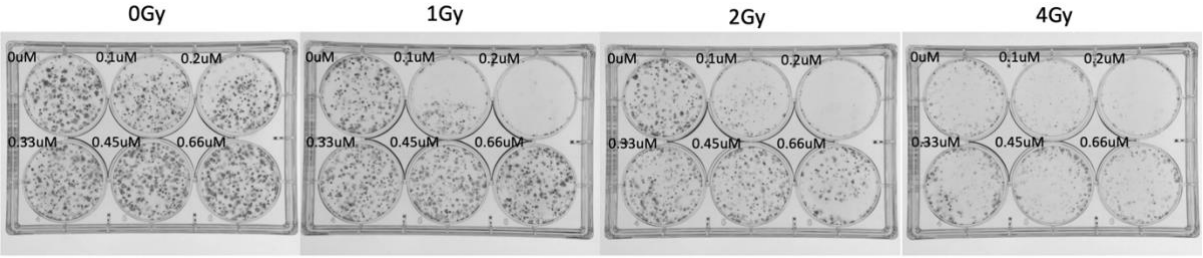

Figure 24. Representative images of clonogenic assays in MiaPaCa-2 cells treated with a combination of BAQ13 and radiation.

cells, representative image seen in Figure 24, had a similar, albeit more irregular trend with significant synergism seen at higher doses of BAQ13 (0.33-0.66μM) and lower doses of radiation (1-2Gy). However, there was some antagonistic areas within the HSA synergy plot (Fig. 25) which should be further investigated in future studies. Again, Bliss and Loewe plotes (data not shown) had similar outputs with similar areas of antagonism and synergy albeit less synergy in the Loewe model. Based on the synergistic potential of these intrinsically radioresistant cells, we decided to expand our screening of this combination to other cell lines with varying degrees and types of radioresistance.

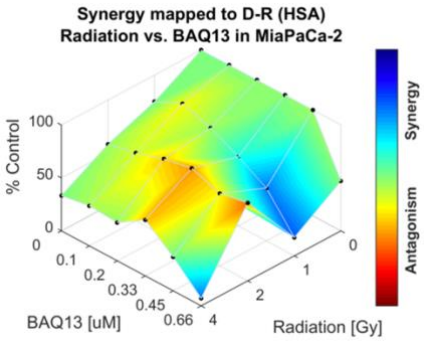

Figure 25. HSA synergy plot of the results of combination treated colony formation assays in MiaPaCa-2 cells.

Glioblastoma Multiforme (GBM)

GL261

GBM is a cancer type commonly plagued by radioresistance. Rather than intrinsic radioresistance, this form of cancer tends to rapidly develop radioresistance after treatments via radiotherapy (13). Therefore, we began to experiment on radioresistant (RR) and wild-type (WT) GL261 cells to determine BAQ13's radiosensitizing potential. We performed the same initial

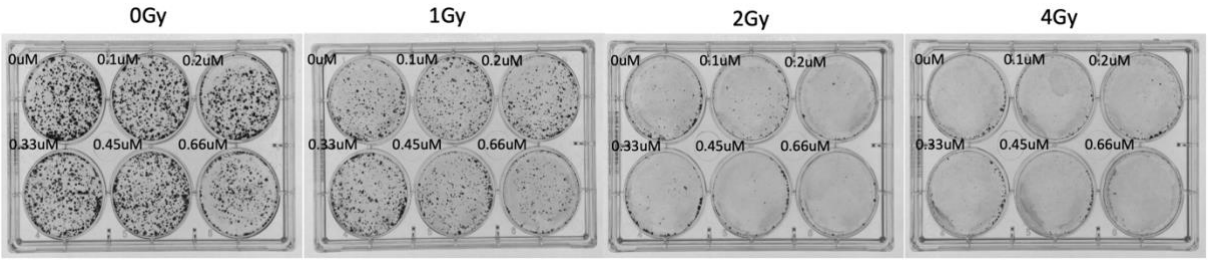

Figure 26. Representative images of clonogenic assays in RR GL261 cells treated with a combination of BAQ13 and radiation.

characterization experiments mentioned in the preceding section to determine chronic BAQ13 and radiation IC_{50}s before combination treatment. As expected, the WT GL261 cells had a lower radiation IC_{50} than the RR GL261 but the sensitivity to BAQ13 was essentially the same regardless of radioresistant status (48-hour IC_{50}s = ~2.5μM). For the combination treatment colony formation assay we utilized the same doses of BAQ13 and radiation as in the previous section for both RR and WT GL261 cells. Figure 26 demonstrates the dose-responsive effect of radiation and BAQ13 in RR GL261 cells which is further supported by the synergy displayed on the HSA synergy plot (Fig. 27) at nearly all doses. The same synergy was also seen in both Bliss and Loewe models (data not shown). The combination treatment was not as synergistic in the

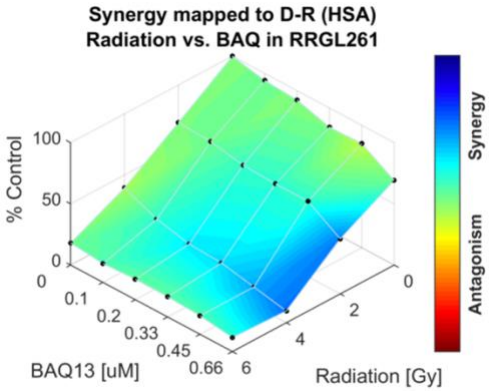

Figure 27. HSA synergy plot of the results of combination treated colony formation assays in RR GL261 cells.

WT GL261 cells (Fig. 28) that, despite a relatively dose-responsive trend, did not show synergy at any doses, except for a slight hint of synergy at the highest dose of BAQ13 and radiation (Fig. 29). Additionally, neither the Bliss nor Loewe models (data not shown) demonstrated any more or less synergy than what is seen in the HSA plot. It is also worth noting that a narrower BAQ13 dose range was used for the WT GL261 colony formation assay (0.2-0.45μM) due to space constraints in the radiation facility. Therefore, it would be worth investigating whether synergy could be achieved at higher doses of BAQ13 for the WT GL261 cells. Overall, these results suggest that BAQ13 has the potential to mitigate radioresistance in cells with acquired radioresistance and further study should include the potential to prevent this radioresistance in wild-type cells.

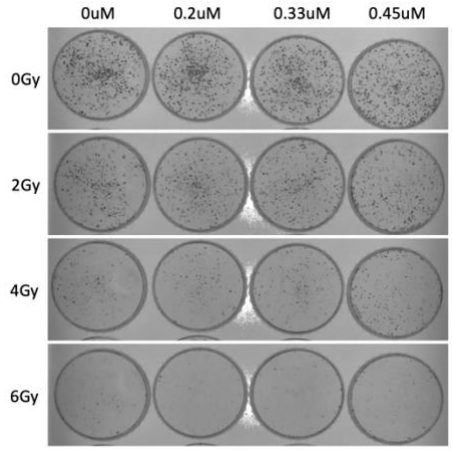

Figure 28. Representative images of clonogenic assays in WT GL261 cells treated with a combination of BAQ13 and radiation.

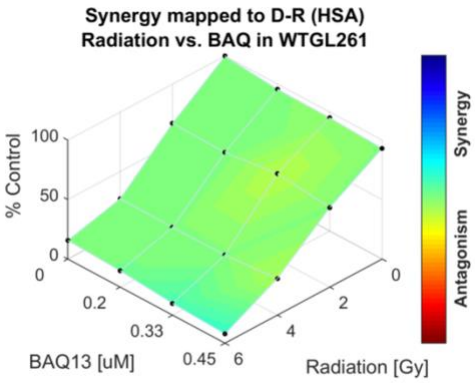

Figure 29. HSA synergy plot of the results of combination treated colony formation assays in WT GL261 cells.

U251

To make conclusions more accurately about the combination's potential in GBM, we expanded our screen to another cell line, U251. Again, we utilized a WT and RR pair for our

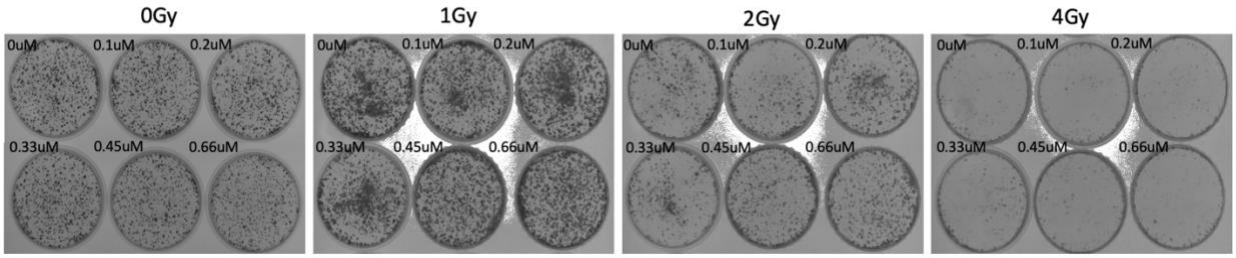

Figure 30. Representative images of clonogenic assays in RR U251 cells treated with a combination of BAQ13 and radiation.

experimentation to determine whether BAQ13 has the ability to lessen or reverse radioresistance. The same initial characterization experiments as detailed previously were performed with WT U251 exhibiting higher sensitivity to radiation as was expected. WT or RR status again did not seem to influence the sensitivity to BAQ13 with the 48-hour IC_{50}s being 2.5 and 2.75µM, respectively. For combination treatment, we utilized the same radiation doses (0-6Gy) and BAQ13 doses (0-0.66µM) as in the GL261 cells for both RR and WT U251. Figure 30 demonstrates that there was a consistent dose-response effect with increasing doses of radiation with a lesser effect seen with increasing doses of BAQ13 in RR U251. However, this did not translate to significant synergy, if any at all with the HSA synergy plot (Fig. 31) showing little to no synergistic areas and Bliss and Loewe models (data not shown) exhibiting very similar results. The small potential for synergy in the RR U251 suggests that further study should include expanded doses of BAQ13 to investigate if a greater dose-response and thus greater synergy can be achieved. Interestingly, the WT U251 had different results with a greater dose-response effect seen with increasing doses of radiation with a lesser trend seen with

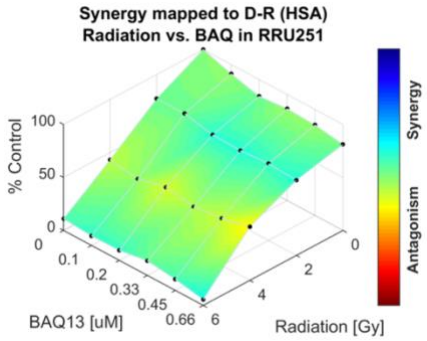

Figure 31. HSA synergy plot of the results of combination treated colony formation assays in RR U251 cells.

increasing doses of BAQ13 seen in Figure 32. The HSA synergy plot for the WT U251 (Fig. 33)

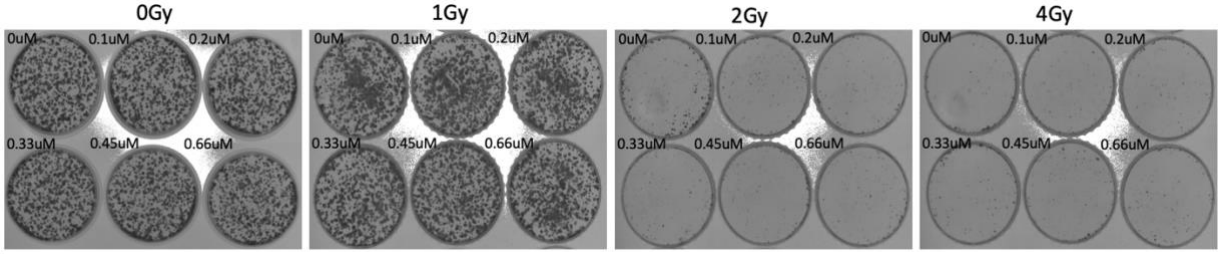

Figure 32. Representative images of clonogenic assays in WT U251 cells treated with a combination of BAQ13 and radiation.

showed synergy at many doses of BAQ13 and at 4Gy radiation with similar if not more synergy seen in both Bliss and Loewe models (data not shown). The synergy seen with WT rather than RR U251 indicates that within the U251 cell line BAQ13 does not have a strong, if any, potential to radiosensitize but may play a role in preventing radioresistance.

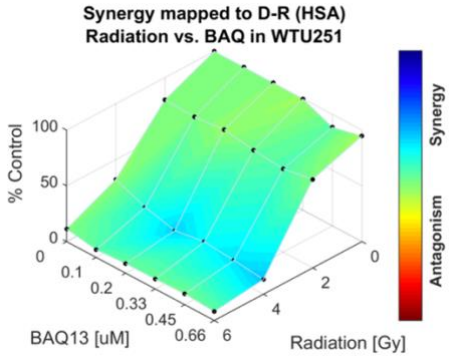

Figure 33. HSA synergy plot of the results of combination treated colony formation assays in WT U251 cells.

Oral Cancer

Oral cancer is another cancer type typically treated with radiotherapy which ultimately leads to the development of acquired radioresistance. Therefore, we decided to include this cancer type as part of our screen to further determine the efficacy of the BAQ13 – radiation combination. For this experiment, we utilized the OSC3 cell line which had a 48-hour BAQ13 IC_{50} of 4.5µM, significantly higher than most

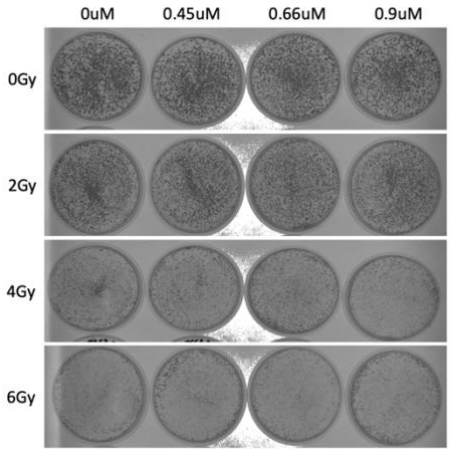

Figure 34. Representative images of clonogenic assays in OSC3 cells treated with a combination of BAQ13 and radiation.

of the cell lines from previous sections. This led us to use a higher BAQ13 dose range (0.45µM - 0.9µM) for combination treatment with radiation doses remaining the same (2-6Gy). The results of this assay revealed a synergistic effect for the combination, particularly at doses at or higher than 2Gy and 0.66µM for radiation and BAQ13, respectively. Other doses demonstrated very slight synergy as seen in the HSA plot (Fig 35) and there was a visible dose-response effect seen with increasing doses of both treatments. This was further supported by Bliss and Loewe model outputs showing the same degree of synergy (data not shown). Thus, OSC3 cells were rendered more sensitive to radiation after combination treatment as evidenced by strong dose-response and synergistic effects. Future study could include expansion of dose ranges and addition of a radioresistant group to determine the radiosensitization ability of the BAQ13 – radiation combination in this cancer type.

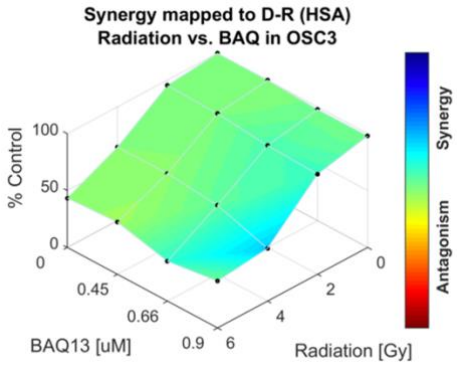

Figure 35. HSA synergy plot of the results of combination treated colony formation assays in OSC3 cells.

Breast Cancer

As one of the more prevalent cancer types, breast cancer is commonly affected by various forms of treatment resistance, including radioresistance (38). To investigate the BAQ13 – radiation combination in this cancer type, we utilized the triple negative breast cancer (TNBC) cell line MDA-MB-231. Characterization experiments revealed a 48-hour BAQ13 IC_{50} of ~2µM, however this cell line was more sensitive to radiation with no growth seen above 4Gy.

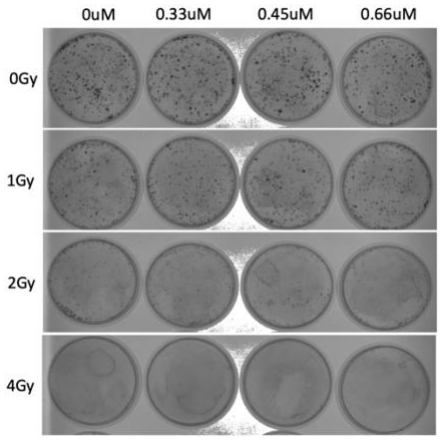

Figure 36. Representative images of clonogenic assays in MDA-MB-231 cells treated with a combination of BAQ13 and radiation.

Therefore, for the combination treatment, the BAQ13 dose range was similar to previous experiments (0.33-0.66μM) and the radiation doses were lower (1, 2, and 4Gy). This revealed very little synergy, despite the visible lack of growth upon increasing doses of each treatment with essentially no growth at the 4Gy dose. In all models (HSA, Bliss, Loewe) the same lack of synergy was observed with both Bliss and Loewe models (data not shown) demonstrating slightly more antagonism. This seems to suggest that the combination is not as effective in MDA-MB-231 cells although each treatment alone proved to be efficacious. Further investigation should include expansion to other breast cancer cell lines, specifically the inclusion of luminal cell lines to determine if the combination is only ineffective in TNBC.

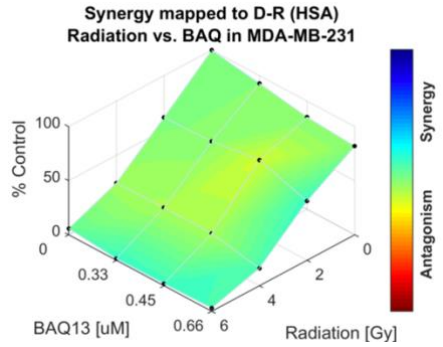

Figure 37. HSA synergy plot of the results of combination treated colony formation assays in MDA-MB-231 cells.

Bladder Cancer

The next cell line screened for combination efficacy was the bladder cancer cell line J82. Again, this cancer type is prone to radioresistance after treatment via radiotherapy which led to its addition to our screen of the BAQ13 – radiation combination. This cell line had a similar 48-hour BAQ13 IC_{50} to some of the previous cell lines (~2μM) with a moderate sensitivity to radiation. Therefore, combination treatment was initiated with BAQ13 doses ranging from 0.2-0.45μM and radiation doses of 2, 4, and 6Gy. This resulted in significant synergy at the high doses of each treatment and slight synergy at lower doses which was

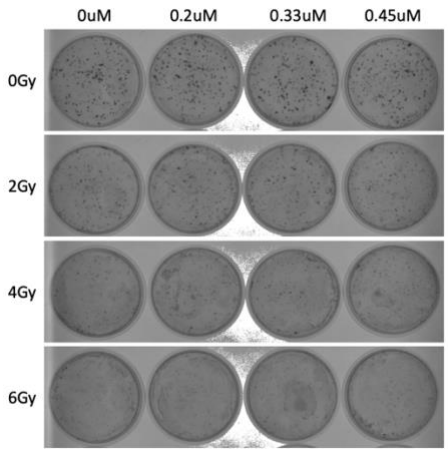

Figure 38. Representative images of clonogenic assays in J82 cells treated with a combination of BAQ13 and radiation.

further supported by a strong dose-response effect with increasing doses of both BAQ13 and radiation. Each model exhibited similar synergy (Bliss and Loewe models not shown) with the HSA and Loewe models demonstrating the highest degrees of synergy. Overall, this suggests that this combination is particularly efficacious in J82 cells and further study should include expansion to other bladder cancer cell lines to determine the extent of its efficacy in this cancer type.

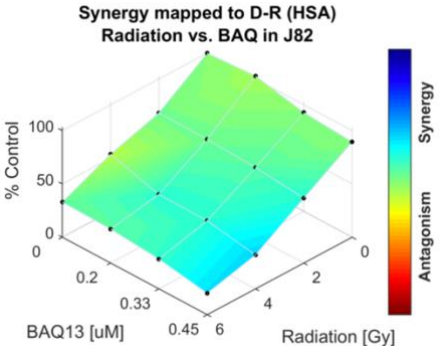

Figure 39. HSA synergy plot of the results of combination treated colony formation assays in J82 cells.

Prostate Cancer

Radiation is commonly utilized in the treatment of prostate cancer. Therefore, this cancer type was added into our screen to determine if BAQ13 has the potential to prevent the inevitable resistance the cancer type will develop to radiation. For our investigation of prostate cancer, we utilized the 22RV1 cell line which demonstrated a 48-hour BAQ13 IC_{50} of 2µM with other initial characterization experiments the same as previously outlined. For combination treatment, we utilized radiation doses 1, 2, and 4Gy and BAQ13 doses 0.2, 0.33, and 0.45µM due to its lower IC_{50}. It is worth noting that for this cell line, the colonies were very small despite a longer incubation for

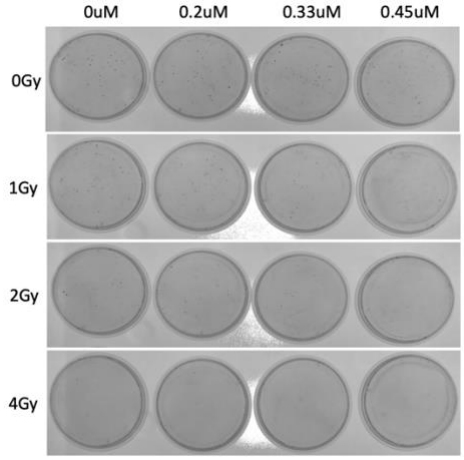

Figure 40. Representative images of clonogenic assays in 22RV1 cells treated with a combination of BAQ13 and radiation.

each colony formation (15 rather than 7-10 days as in previous experiments). For the combination colony formation (Fig. 40) there was a significant dose-response effect with increasing doses of both radiation and BAQ13 with very few colonies seen at 4Gy. The HSA synergy plot seen in Figure 41 supports this by demonstrating synergy at 1Gy and 0.33μM BAQ13 despite some antagonism at low doses of BAQ13 and high doses of radiation. Bliss and Loewe models (data not shown) had similar outputs with slightly less synergy seen in the Bliss model. All of this suggests that this combination has potential in prostate cancer, however the minor antagonism should be further investigated. Further study should also include the expansion to other prostate cancer cell lines to determine if the combination can be more efficacious.

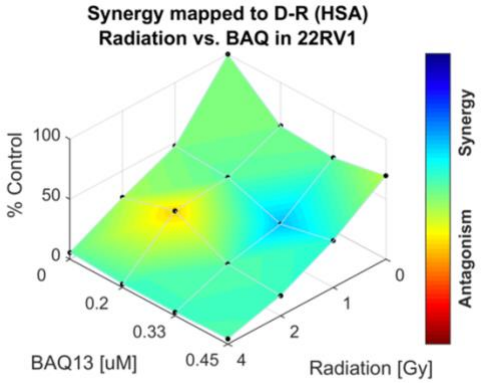

Figure 41. HSA synergy plot of the results of combination treated colony formation assays in 22RV1 cells.

Discussion

Pharmacological Manipulation of Ferroptosis in Combination with BAQ13

Targeting ferroptosis has become an attractive method to induce cancer cell death. Specifically, induction of this recently discovered cell death pathway has proven efficacious, leading us to investigate whether the addition of our lab's autophagy inhibitor, BAQ13, would enhance the cytotoxicity of ferroptosis inducers in MiaPaCa-2 cells. Erastin, which activates p53 to induce ferroptosis, had strong synergistic potential with BAQ13 as evidenced by the HSA plot in Figure 4. However, the same degree of synergy was not achievable with the combination of BAQ13 and RSL3 which triggers ferroptosis by directly inhibiting GPX4. Multiple attempts (Fig. 5, 6) with different dose ranges and incubation periods yielded minimal, if any, synergy with nothing comparable to Erastin's results. This seems to indicate that BAQ13 is only synergistic with ferroptosis inducers employing Erastin's mechanism of activating p53 rather than RSL3's inhibition of GPX4. Future investigation should include other ferroptosis inducers or anticancer compounds that activate p53 to determine the extent of this combination's efficacy.

We next performed a western blot using MiaPaCa-2 cells to further understand the cell death pathways other than autophagy and ferroptosis that are implicated in this combination. Treatment groups included BAQ13 only, Erastin only, combination treatment, and chloroquine and napabucasin controls for autophagy and apoptosis. The results of this and other attempts were inconsistent, but the main effects were seen within the combination group. It appears that combination treatment induced an upregulation of RIP3 but not MLKL despite RIP3's regulatory role over the latter protein. This suggests some involvement of necrosis in this combination as MLKL was still expressed, albeit not as strongly as in other groups. PARP was also cleaved in the combination treated groups which highlights involvement of apoptosis in this combination.

Overall, this data suggests that the Erastin – BAQ13 combination has significant synergistic potential and potentially induces multiple cell death pathways outside of ferroptosis and autophagy. This combination should be further studied in other pancreatic cell lines and cancer types as well as mechanistically investigated to determine the reasons behind this combination's synergy.

Paclitaxel -BAQ13 Combination to Address Autophagic Resistance Mechanisms

PTX is a commonly used chemotherapeutic agent to combat tumor growth in multiple cancer types. However, its commonality has led to widespread treatment resistance with autophagy being implicated as one of the resistance mechanisms. Therefore, it seemed prudent to attempt combination therapy with our lab's autophagy inhibitor, BAQ13, to target this subset of treatment resistance and enhance PTX's cytotoxicity. Pancreatic cancer cells have elevated levels of autophagy so they should theoretically be more resistant to PTX treatment so to assess its toxicity alone, we treated PANC-1 and MiaPaCa-2 cells with concentrations ranging from 0-10μM. None of these concentrations led to major cytotoxicity below 50% which could be due to the cytostatic nature of PTX but could also be due to an inherent resistance in these pancreatic cancer cells.

The lack of toxicity with PTX alone further supported the idea of combination treatment with BAQ13 to attempt to enhance PTX's efficacy in these pancreatic cancer cells. We performed several attempts with this combination with different doses of PTX as well as different incubation periods which all yielded different results and varying degrees of synergy. The most synergy was seen with simultaneous co-treatment of BAQ13 and PTX for 72 hours for both cell lines which led us to try alternative approaches to try and achieve greater synergism. Unfortunately, none of the other treatment paradigms led to greater synergy with some even

leading to antagonistic effects, especially with 24-hour pretreatment with BAQ13. PANC-1 cells exhibited the most consistent synergy across attempts and treatment paradigms but there was still major inconsistencies and antagonism with certain pretreatments and incubation times. Therefore, lack of replication of synergy suggests that this combination has potential in pancreatic cancer cells but should be further investigated. Specifically, more expansion of dose ranges of each compound should be attempted, especially for the treatment paradigms that led to the most synergy. It would also be prudent to attempt this combination in other cancer types, perhaps some with lower levels of autophagy as that may modulate the efficacy of PTX as well as the PTX – BAQ13 combination.

BAQ13's Manipulation of Metabolism and Lipid Toxicity

It has been established that abnormal FAO activity is linked to oncogenesis due to cancer cell reliance on this process for proliferation, survival, metastasis, and more (23). Therefore, we decided to investigate BAQ13's ability to modulate this subset of metabolism to determine mechanisms other than autophagy that may be responsible for its cytotoxicity. As part of this investigation, we measured dose- and time-dependent changes in FAO activity upon treatment with varying concentrations of BAQ13 in PANC-1 and MiaPaCa-2 cells. The results of multiple attempts did not yield a stereotypical trend with no dose- or time-dependent increase or decrease in FAO activity. Instead, we observed an upregulation of FAO activity with low doses of BAQ13 compared to baseline activity in the untreated control. This was followed by a "crash" in FAO activity with increasing doses of BAQ13 for both cell lines. Additionally, time-dependent changes were negligible, showcasing the same trend seen across BAQ13 doses. We also included a chloroquine control which consistently demonstrated similar or increased FAO activity compared to high doses of BAQ13. Overall, this data suggests that at low doses, BAQ13

increases FAO activity, perhaps by increasing cell stress and reliance on this metabolic pathway rather than glycolysis. Then, with increasing concentrations there is a sharp decrease in FAO activity suggesting BAQ13 is either capable of inhibiting FAO or that cell death/senescence is rendering metabolism unnecessary. To verify or further investigate these results, other methods of measuring FAO activity should be employed in addition to western blots to determine the mechanisms behind BAQ13's modulation of this metabolic process.

As BAQ13's manipulation of FAO was made clear by the preceding data, we sought to investigate the addition of FAO inhibitor Etomoxir (ETX) to our experiments. ETX's mechanism of action is inhibition of CPT1, a key regulator of FAO and an attractive therapeutic target for cancer treatment. Published studies have showcased ETX's ability to impair NADPH production and increase ROS which ultimately leads to depletion of ATP and cell death (30). Therefore, we set out to both investigate its ability to combine and potentially synergize with BAQ13 as well as utilize ETX as a control in our studies of FAO activity. Initial characterization using PANC-1 and MiaPaCa-2 cells revealed a very high IC_{50} of 300-400μM for each cell line which is supported by publications utilizing ETX (34). However, while combination treatment with BAQ13 did substantially lower the viability of the pancreatic cancer cells, reducing the IC_{50} to 100-200μM, there wasn't significant cytotoxicity and therefore no synergy with this combination. Thus, we relegated use of ETX to FAO activity-related experiments as a control. We then began to measure FAO using a fluorescent dye, FAOBlue, with 4 treatment groups in PANC-1 cells: no treatment, low dose BAQ13, high dose BAQ13, and ETX. Overnight treatment in a second attempt led to a trend similar to what was discussed previously with the low dose of BAQ13 upregulating FAO activity compared to the untreated control with a decrease in activity at the high dose of BAQ13 sometimes comparable to the ETX group which had very

little, if any, FAO activity. This further supports the previous results and suggests that ETX should be further investigated in other pancreatic cancer cells or cancer types to determine if it is capable of synergizing with BAQ13 or other compounds. Additionally, future work should focus on the effects of FAO modulation by BAQ13 as well as ETX on other metabolic and cellular processes.

Lastly, due to BAQ13's ability to modulate FAO, we questioned its ability to induce lipid disorder and toxicity. To visualize these effects, we employed several fluorescent dyes in PANC-1 cells, the first being LipiDYE-M which was used to detect the presence of lipid droplets via a shift from green to red fluorescence. For all dyes, we utilized the same treatment groups and incubation periods described for the FAOBlue experiments. As shown in Figure 19, increasing doses of BAQ13 led to an increase in red color, especially visible in the 63X oil lens images. This indicates increased lipid toxicity which was not seen in the untreated or ETX groups. It is worth noting that this dye is also able to detect morphological changes in organelles through differences in fluorescent color, however, PANC-1 cells have a very limited cytoplasm making this very difficult. We next used LipiORDER dye to visualize changes in membrane lipid order via changes in fluorescence from green (low polarity, ordered bilayer) to red (high polarity, disordered bilayer). Again, increasing doses of BAQ13 led to an increase in red fluorescence and decrease in green fluorescence compared to the more balanced, untreated control exhibiting green/yellow fluorescence with ETX demonstrating a slight shift towards disorder as evidenced by orange fluorescence (Fig. 20). Therefore, this supports the conclusions made about LipiDYE-M with BAQ13 inducing disordered lipid bilayers in addition to lipid droplets. Lastly, we utilized LipidTOX, a dye developed to detect phospholipidosis via increased green fluorescence. The results of this dye further supported what was observed in the previous imaging

experiments; increased BAQ13 led to increased phospholipidosis made evident by an increase in green fluorescence, especially compared to the untreated control, with ETX showing minimal green fluorescence (Fig. 21). Overall, this set of experiments showcases BAQ13's ability to not only manipulate FAO but induce various forms of lipid toxicity and disorder in cancer cells. More studies should be executed to determine the implications of this disorder on other cellular processes and cell death pathways as well as the mechanisms behind it and its interactions with metabolism.

BAQ13 and Radiotherapy Combination to Combat Radioresistance

Radiotherapy's prevalence as a cancer treatment has led radioresistance to become a significant issue with many patients developing resistance and recurrence of their cancer after radiation treatment. Radiation is a source of cell stress that leads to the induction of autophagy with specific induction of cytoprotective autophagy rather than cell death. This led to the hypothesis that inhibition of autophagy by BAQ13 in combination with radiation would enhance the efficacy of each treatment. Additionally, we sought to determine whether this combination could lessen, prevent, or even reverse radioresistance through testing cell lines with intrinsic radioresistance due to upregulated autophagy such as pancreatic cancer cells as well as cells with acquired radioresistance after repeated exposure. We began with combination treatment in pancreatic cancer cell lines MiaPaCa-2 and PANC-1 via clonogenic assays which yielded a visible dose-response effect with increasing doses of both radiation and BAQ13 (Fig. 22, 24). To assess the synergistic potential of this combination we relied on Combenefit synergy software which revealed synergy in both cell lines with PANC-1 having a more consistent increase in synergy with increasing doses of each treatment and MiaPaCa-2's synergy being more sporadic in the lower doses of BAQ13 and higher doses of radiation. Overall, this indicates that this

combination has potential in cancer types possessing intrinsic radioresistance as it seemed to enhance the efficacy of each treatment as evidenced by both the dose-response effect and synergism.

The potential the pancreatic cancer cell lines demonstrated with the combination led us to investigate its efficacy in cells with acquired radioresistance. Namely we utilized GBM cell lines as this cancer type is very commonly treated with radiation and is thus extremely affected by radioresistance. For this line of experimentation, we used wilt-type (WT) and radioresistant (RR) pairs of GL261 and U251 cell lines for the same clonogenic assays as discussed above. There was a strong dose-response effect seen in both cell lines with the RR GL261 demonstrating a bigger effect which was supported by the strong synergy seen throughout all doses. The WT GL261 was more sensitive to radiation but did not exhibit significant synergy at any doses. This seems to suggest that RR cells are more susceptible to this combination treatment which could potentially indicate the ability of the BAQ13 – radiation combination to lessen radioresistance. However, the results of the combination treatment on RR and WT U251 cells did not support this conclusion with less synergy seen in RR than WT cells. These opposing results do not permit for an overarching conclusion about this combination in GBM cells but does demonstrate the potential for BAQ13 to have synergistic effects in these cells. Despite the appearance of synergy in RR GL261 but WT U251, there is still an implication that the BAQ13 – radiation combination can prevent resistance. The capability of the combination to lessen or reverse resistance should be further investigated, especially in GL261 cells as the strongest synergy was seen in RR cells.

Due to the synergism seen in cell lines with intrinsic and acquired radioresistance we decided to perform a screen on other cancer types that are treated with radiation. First, we screened oral cancer using the OSC3 cell line which demonstrated a dose-dependent decrease in

colony number with increasing doses of each treatment (Fig. 34). This was supported by the synergy seen in the HSA plot in Figure 35 which showed mild to moderate synergy at higher doses of BAQ13 and almost all doses of radiation. Next, we screened breast cancer using the triple negative breast cancer (TNBC) MDA-MB-231 cell line. Again, there was a visible dose-response effect, albeit to a lesser degree than the previously discussed cell lines, with increasing doses (Fig. 36), however, the HSA synergy plot seen in Figure 37 did not display any significant synergy with this cell line. To further investigate the combination in breast cancer, it may be necessary to expand to other cell lines and potentially investigate luminal cell lines rather than TNBC. The next cancer type we chose to screen was bladder cancer using the J82 cell line. This cell line exhibited a strong dose-response effect, especially with increasing doses of radiation (Figure 38). This was supported by the HSA synergy plot in Figure 39 which showcased mild to moderate synergy at nearly all doses. The last cancer type that was screened was prostate cancer using the 22RV1 cell line. Despite its smaller colonies, this cell line also exhibited a strong dose response effect with increasing doses of both BAQ13 and radiation (Fig. 40). The corresponding HSA synergy plot (Fig. 41) supported this by illustrating synergy at high doses of BAQ13 and low doses of radiation. For this cell line, further study should focus on these doses and investigate the slight antagonism seen at high doses of radiation and low doses of BAQ13.

Overall, this data suggest that this combination has significant potential in many cancer types with particularly strong synergy seen in cells with intrinsic or acquired radioresistance. Therefore, the potential of this compound to reverse radioresistance should be explored especially as a lot of current research is investigating radiosensitizers. Additionally, future studies following this line of experimentation should include western blots to visualize the induction of autophagy by radiation and subsequent inhibition by BAQ13 to pinpoint the

mechanism more accurately behind this synergistic combination. Eventually this should also progress to *in vivo* studies to determine if this combination remains effective in a more complex model.

Conclusion

Based upon the preceding data, it is clear that BAQ13 has significant potential to synergize with a variety of treatment modalities. First, BAQ13 demonstrated its ability to synergize with ferroptosis inducer Erastin but not RSL3. This could be due to different mechanisms of action or that we were unable to discern the ideal dose ranges for each compound. There was also some potential for synergy seen with the BAQ13 – PTX combination despite the fact that some of the treatment paradigms were plagued by antagonism. Future study of this combination should include expanded dose ranges, specifically within the incubation times that yielded the most synergy. BAQ13 did not show the same potential with FAO inhibitor Etomoxir but the same line of experimentation revealed BAQ13's ability to potentially inhibit FAO and induce various forms of lipid toxicity and bilayer disorder. Lastly, the combination with the most potential for synergy was BAQ13 and radiation which led us to expand past the pancreatic cancer cell lines used for the other combinations. This revealed the potential for BAQ13 to both lessen and prevent radioresistance in many cancer types plagued by acquired or intrinsic radioresistance.

For the radiation – BAQ13 combination to become clinically applicable, there are several studies to be completed. First, mechanistic studies should be executed to both outline the mechanism of action of BAQ13 alone and in combination with radiation. As the rationale for this combination centers around BAQ13's autophagy inhibition, there should be visualization of radiation alone inducing autophagy with combination treatment leading to its inhibition. With the mechanism outlined, this combination should also be tested in an animal model to determine whether its efficacy is retained in a more complex system. All of this will provide a solid foundation for this combination to eventually be considered for clinical application, especially

once BAQ13 gains approval. The prevalence of radioresistance in the clinic highlights a need for a combination such as this with BAQ13's targeting of autophagy and lysosomal disruption rather than commonly targeted cell death pathways only enhancing its attractiveness. With many future studies to be completed with collaborations across disciplines, this combination could prove very useful to combat radioresistance through either its prevention or attenuation.

References

1. Kim BM, Hong Y, Lee S, et al. Therapeutic Implications for Overcoming Radiation Resistance in Cancer Therapy. *Int J Mol Sci*. 2015;16(11):26880-26913. Published 2015 Nov 10. doi:10.3390/ijms161125991 PMID: 26569225
2. Tam SY, Wu VW, Law HK. Influence of autophagy on the efficacy of radiotherapy. *Radiat Oncol*. 2017;12(1):57. Published 2017 Mar 21. doi:10.1186/s13014-017-0795-y PMID: 28320471
3. Ma Z, Li J, Lin K, et al. Author Correction: Pharmacophore hybridisation and nanoscale assembly to discover self-delivering lysosomotropic new-chemical entities for cancer therapy. *Nat Commun*. 2021;12(1):2013. Published 2021 Mar 25. doi:10.1038/s41467-021-22419-2
PMID: 33767181
4. Chen H, Han Z, Luo Q, et al. Radiotherapy modulates tumor cell fate decisions: a review. *Radiat Oncol*. 2022;17(1):196. Published 2022 Dec 1. doi:10.1186/s13014-022-02171-7
PMID: 36457125
5. de Mey S, Dufait I, De Ridder M. Radioresistance of Human Cancers: Clinical Implications of Genetic Expression Signatures. *Front Oncol*. 2021;11:761901. Published 2021 Oct 27. doi:10.3389/fonc.2021.761901
PMID: 34778082
6. Galeaz C, Totis C, Bisio A. Radiation Resistance: A Matter of Transcription Factors. *Front Oncol*. 2021;11:662840. Published 2021 Jun 1. doi:10.3389/fonc.2021.662840
PMID: 34141616
7. Han MW, Lee JC, Choi JY, et al. Autophagy inhibition can overcome radioresistance in breast cancer cells through suppression of TAK1 activation. *Anticancer Res*. 2014;34(3):1449-1455.
PMID: 24596393
8. Zhang X, Wang J, Li X, Wang D. Lysosomes contribute to radioresistance in cancer. *Cancer Lett*. 2018;439:39-46. doi:10.1016/j.canlet.2018.08.029
PMID: 30217567
9. Oike T, Ohno T. Molecular mechanisms underlying radioresistance: data compiled from isogenic cell experiments. *Ann Transl Med*. 2020;8(6):273. doi:10.21037/atm.2020.02.90
PMID: 32355717
10. Stackhouse CT, Anderson JC, Yue Z, et al. An in vivo model of glioblastoma radiation resistance identifies long noncoding RNAs and targetable kinases. *JCI Insight*. 2022;7(16):e148717. Published 2022 Aug 22. doi:10.1172/jci.insight.148717
PMID: 35852875
11. Jing D, Jiang N, Wang F, et al. Nanoradiosensitizer with good tissue penetration and enhances oral cancer radiotherapeutic effect. *Biomaterials*. 2022;289:121769. doi:10.1016/j.biomaterials.2022.121769
PMID: 36084485
12. De Ruysscher D, Niedermann G, Burnet NG, Siva S, Lee AWM, Hegi-Johnson F. Radiotherapy toxicity [published correction appears in Nat Rev Dis Primers. 2019 Mar

4;5(1):15]. *Nat Rev Dis Primers*. 2019;5(1):13. Published 2019 Feb 21. doi:10.1038/s41572-019-0064-5
PMID: 30792503
13. Jiang N, Xie B, Xiao W, et al. Fatty acid oxidation fuels glioblastoma radioresistance with CD47-mediated immune evasion. *Nat Commun*.2022;13(1):1511.Published 2022 Mar 21. doi:10.1038/s41467-022-29137-3
PMID: 35314680
14. Valanciunaite J, Kempf E, Seki H, et al. Polarity Mapping of Cells and Embryos by Improved Fluorescent Solvatochromic Pyrene Probe. *Anal Chem*. 2020;92(9):6512-6520. doi:10.1021/acs.analchem.0c00023
PMID: 32153188
15. Rehman A, Hemmert KC, Ochi A, et al. Role of fatty-acid synthesis in dendritic cell generation and function. *J Immunol*. 2013;190(9):4640-4649. doi:10.4049/jimmunol.1202312
PMID: 23536633
16. Kajiwara K, Osaki H, Greßies S, et al. A negative-solvatochromic fluorescent probe for visualizing intracellular distributions of fatty acid metabolites. *Nat Commun*. 2022;13(1):2533. Published 2022 May 9. doi:10.1038/s41467-022-30153-6
PMID: 35534485
17. Vasquez KO, Casavant C, Peterson JD. Quantitative whole body biodistribution of fluorescent-labeled agents by non-invasive tomographic imaging. *PLoS One*. 2011;6(6):e20594. doi:10.1371/journal.pone.0020594
PMID: 21731618
18. Montelius M, Ljungberg M, Horn M, Forssell-Aronsson E. Tumour size measurement in a mouse model using high resolution MRI. *BMC Med Imaging*. 2012;12:12. Published 2012 May 30. doi:10.1186/1471-2342-12-12
PMID: 22647088
19. Li R, Ran R, Li Q, Huang Y, Gu Y, Si D. Development of an LC-MS/MS method for the quantitation of deoxyglycychloxazol in rat plasma and its application in pharmacokinetic study. *J Pharm Anal*. 2016;6(3):184-189. doi:10.1016/j.jpha.2016.03.002
PMID: 29403980
20. McArthur K, Kile BT. Apoptotic mitochondria prime anti-tumour immunity. *Cell Death Discov*. 2020;6(1):98. Published 2020 Oct 7. doi:10.1038/s41420-020-00335-6
PMID: 33083019
21. Jiang X, Stockwell BR, Conrad M. Ferroptosis: mechanisms, biology and role in disease. Nat Rev Mol Cell Biol. 2021;22(4):266-282.
22. Du J, Wang X, Li Y, et al. DHA exhibits synergistic therapeutic efficacy with cisplatin to induce ferroptosis in pancreatic ductal adenocarcinoma via modulation of iron metabolism. *Cell Death Dis*. 2021;12(7):705. Published 2021 Jul 15. doi:10.1038/s41419-021-03996-y
23. Ma, Y., Temkin, S. M., Hawkridge, A. M., Guo, C., Wang, W., Wang, X. Y., & Fang, X. (2018). Fatty acid oxidation: An emerging facet of metabolic transformation in cancer. *Cancer letters*, *435*, 92–100. https://doi.org/10.1016/j.canlet.2018.08.006

24. Carracedo, A., Cantley, L. C., & Pandolfi, P. P. (2013). Cancer metabolism: fatty acid oxidation in the limelight. *Nature reviews. Cancer*, *13*(4), 227–232. https://doi.org/10.1038/nrc3483
25. Tung S, Shi Y, Wong K, Zhu F, Gorczynski R, Laister RC, Minden M,Blechert AK, Genzel Y, Reichl U, Spaner DE, PPARalpha and fatty acid oxidation mediate glucocorticoid resistance in chronic lymphocytic leukemia, *Blood* 122 (2013) 969–980.
26. Barger JF, Gallo CA, Tandon P, Liu H, Sullivan A, Grimes HL, Plas DR, S6K1 determines the metabolic requirements for BCR-ABL survival, *Oncogene* 32 (2013) 453–461.
27. Shinohara H, Kumazaki M, Minami Y, Ito Y, Sugito N, Kuranaga Y,Taniguchi K, Yamada N, Otsuki Y, Naoe T, Akao Y, Perturbation of energy metabolism by fatty-acid derivative AIC-47 and imatinib in BCR-ABL-harboring leukemic cells, *Canc. Lett* 371 (2016) 1–11.
28. Kitajima S, Yoshida A, Kohno S, Li F, Suzuki S, Nagatani N, Nishimoto Y,Sasaki N, Muranaka H, Wan Y, Thai TC, Okahashi N, Matsuda F, Shimizu H,Nishiuchi T, Suzuki Y, Tominaga K, Gotoh N, Suzuki M, Ewen ME,Barbie DA, Hirose O, Tanaka T, Takahashi C, The RB-IL-6 axis controls self-renewal and endocrine therapy resistance by fine-tuning mitochondrial activity, *Oncogene* 36 (2017) 5145–5157.
29. Yao, C. H., Liu, G. Y., Wang, R., Moon, S. H., Gross, R. W., & Patti, G. J. (2018). Identifying off-target effects of etomoxir reveals that carnitine palmitoyltransferase I is essential for cancer cell proliferation independent of β-oxidation. *PLoS biology*, *16*(3), e2003782. https://doi.org/10.1371/journal.pbio.2003782
30. Qu, Q., Zeng, F., Liu, X. *et al.* Fatty acid oxidation and carnitine palmitoyltransferase I: emerging therapeutic targets in cancer. *Cell Death Dis* **7**, e2226 (2016). https://doi.org/10.1038/cddis.2016.132
31. Škubník J, Svobodová Pavlíčková V, Ruml T, Rimpelová S. Autophagy in cancer resistance to paclitaxel: Development of combination strategies. *Biomed Pharmacother*. 2023;161:114458. doi:10.1016/j.biopha.2023.114458
32. Galletti E, Magnani M, Renzulli ML, Botta M. Paclitaxel and docetaxel resistance: molecular mechanisms and development of new generation taxanes. *ChemMedChem*. 2007;2(7):920-942. doi:10.1002/cmdc.200600308
33. Luongo M, Marinelli O, Zeppa L, et al. Cannabidiol and Oxygen-Ozone Combination Induce Cytotoxicity in Human Pancreatic Ductal Adenocarcinoma Cell Lines. *Cancers (Basel)*. 2020;12(10):2774. Published 2020 Sep 27. doi:10.3390/cancers12102774
34. O'Connor, R.S., Guo, L., Ghassemi, S. *et al.* The CPT1a inhibitor, etomoxir induces severe oxidative stress at commonly used concentrations. *Sci Rep* **8**, 6289 (2018). https://doi.org/10.1038/s41598-018-24676-6
35. Uchinomiya, S., Matsunaga, N., Kamoda, K., Kawagoe, R., Tsuruta, A., Ohdo, S., & Ojida, A. (2020). Fluorescence detection of metabolic activity of the fatty acid beta oxidation pathway in living cells. *Chemical Communications*, *56*(20), 3023-3026. https://doi.org/10.1039/c9cc09993j
36. Di Veroli GY, Fornari C, Wang D, et al. Combenefit: an interactive platform for the analysis and visualization of drug combinations. *Bioinformatics*. 2016;32(18):2866-2868. doi:10.1093/bioinformatics/btw230
37. Keith R. Porter Imaging Facility. *Determining fluorescence intensity and signal*. UMBC. https://kpif.umbc.edu/image-processing-resources/imagej-fiji/determining-fluorescence-intensity-and-positive-signal/

38. Gray, M., Turnbull, A.K., Ward, C. *et al.* Development and characterisation of acquired radioresistant breast cancer cell lines. *Radiat Oncol* **14**, 64 (2019). https://doi.org/10.1186/s13014-019-1268-2